Harmful Algae 118 (2022) 102296

Contents lists available at ScienceDirect

Harmful Algae

journal homepage: www.elsevier.com/locate/hal

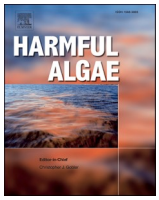

Development, calibration, and evaluation of a model of *Pseudo-nitzschia* and domoic acid production for regional ocean modeling studies

Allison R. Moreno [a,*], Clarissa Anderson [b], Raphael M. Kudela [c], Martha Sutula [d], Christopher Edwards [c], Daniele Bianchi [a]

[a] Atmospheric and Oceanic Sciences Department, University of California Los Angeles, Box 951565, Los Angeles 90095-1565, CA, USA
[b] Southern California Coastal Ocean Observing System, Scripps Institution of Oceanography, La Jolla, CA, USA
[c] Ocean Sciences Department, University of California Santa Cruz, Santa Cruz, CA, USA
[d] Southern California Coastal Water Research Project Authority, Costa Mesa, CA, USA

ARTICLE INFO

Edited by Dr. C. Gobler.

Keywords:
Pseudo-nitzschia
Domoic acid
Ecosystem modeling
Mechanistic Modeling

ABSTRACT

Pseudo-nitzschia species are one of the leading causes of harmful algal blooms (HABs) along the western coast of the United States. Approximately half of known *Pseudo-nitzschia* strains can produce domoic acid (DA), a neurotoxin that can negatively impact wildlife and fisheries and put human life at risk through amnesic shellfish poisoning. Production and accumulation of DA, a secondary metabolite synthesized during periods of low primary metabolism, is triggered by environmental stressors such as nutrient limitation. To quantify and estimate the feedbacks between DA production and environmental conditions, we designed a simple mechanistic model of *Pseudo-nitzschia* and domoic acid dynamics, which we validate against batch and chemostat experiments. Our results suggest that, as nutrients other than nitrogen (i.e., silicon, phosphorus, and potentially iron) become limiting, DA production increases. Under Si limitation, we found an approximate doubling in DA production relative to N limitation. Additionally, our model indicates a positive relationship between light and DA production. These results support the idea that the relationship with nutrient limitation and light is based on direct impacts on *Pseudo-nitzschia* biosynthesis and biomass accumulation. Because it can easily be embedded within existing coupled physical-ecosystem models, our model represents a step forward toward modeling the occurrence of *Pseudo-nitzschia* HABs and DA across the U.S. West Coast.

1. Introduction

Pseudo-nitzschia are one of the leading causes of harmful algal blooms (HABs) along the western coast of the United States. They can produce domoic acid (DA), a neurotoxin that has been shown to negatively impact wildlife, fisheries, and put human life at risk through amnesic shellfish poisoning (Lelong et al., 2012). Half of known *Pseudo-nitzschia* strains have been shown to produce DA at potentially toxic levels; however, under ideal conditions it is possible that all *Pseudo-nitzschia* strains will produce DA (Bates et al., 1998, 2018; Thessen et al., 2009). Understanding the inducing mechanism(s) that result in toxic DA accumulation has been the focus of much HAB research to date and is essential to supporting ecosystem conservation and management of marine resources (Lelong et al., 2012).

While several experiments have identified factors that appear to trigger DA production by *Pseudo-nitzschia* in laboratory cultures, the mechanisms behind this production, and their expression in the oceanic environment remain unclear (Buck, 1992; Garrison et al., 1992; Lelong et al., 2012). Intracellular DA content from laboratory experiments has been shown to be enhanced under phosphorus (P) or silicic acid (Si) limitation (Bates et al., 1991; Fehling et al., 2004; Pan et al., 1996) and DA production appears to increase during periods of reduced primary metabolism. However, along the U.S. West Coast, intense *Pseudo-nitzschia* blooms are commonly found in cool upwelling regions and waters near river outlets. These areas are typically characterized by high nutrient concentrations and elevated primary production. Under nutrient limitation, while blooms are declining, cells can no longer divide but are still harvesting energy from photosynthesis that can be utilized to synthesize secondary metabolites like DA (Pan et al., 1998).

Nutrient stress has been shown to induce DA production and accumulation. P limitation could act as a physiological mechanism to induce elevated levels of DA production. A strong positive relationship exists

* Corresponding author.
E-mail address: allimoreno@atmos.ucla.edu (A.R. Moreno).

https://doi.org/10.1016/j.hal.2022.102296
Received 19 April 2022; Received in revised form 22 July 2022; Accepted 1 August 2022
Available online 11 August 2022

between DA production and alkaline phosphatase activity, an indicator of P limitation (Pan et al., 1996). Consistently, DA synthesis and production is dampened by the addition of inorganic P in cultures (Pan et al., 1998). Si limitation has also been shown to have a strong positive relationship with DA concentrations (Anderson et al., 2006). In diatoms, Si limitation can impede the progression of cell division by stopping the cell in G2 phase during which the cell is preparing for mitosis (Brzezinski, 1992). Si limitation results in decreasing primary metabolism, i.e., DNA synthesis and gene expression, relieving energy for DA production. N limitation is rare along the U.S. West Coast and therefore not expected to impact *Pseudo-nitzschia* to a substantial degree. N limitation has been theorized to inhibit DA production because of an insufficient pool of available cellular N, required to supply ammonium for DA synthesis (Pan et al., 1998). In contrast to these hypotheses, Kudela et al. (2004) and Calu et al. (2009) have shown that in laboratory experiments under severe N limitation, low levels of DA are still produced, perhaps reflective of the relatively low nitrogen requirement for DA synthesis. Thus, it appears that DA production and accumulation are stimulated by general macronutrient stress, with P and Si limitation inducing more effective DA synthesis, and N limitation inhibiting it, although not completely.

DA production could also be encouraged under conditions that reflect trace metal stress. Rue and Bruland (2001) found that DA, when binding with iron (Fe) and copper (Cu), exhibits structural similarities to mugineic acid, a phytosiderophore. Phytosiderophores are low-molecular weight chelators released by cells under Fe stress to increase Fe uptake. Although siderophores are typically specific to iron, Rue and Bruland (2001) found that Cu could also be taken up under Cu limitation by siderophores. In *P. multiseries* and *P. australis* clones isolated from Monterey Bay, California, DA production increased in cultures limited by Fe and Cu (Maldonado et al., 2002). There are two main forms of Cu stress: extreme limitation and toxicity. Rapid increases in Cu have been shown to positively impact DA production (Ladizinsky, 2003). Cellular DA partitioning was previously found to be controlled by the biosynthetic processes rather than an involuntary leakage due to cellular membrane damage (Wells et al., 2005). Thus, a decrease in Fe, or Cu limitation, and/or an increase in Cu availability (Ladizinsky, 2003) could lead to an increase in dissolved DA in the environment and could enhance the severity of DA transfer up the food chain. While the evidence for effects of trace metal limitation and DA production and toxicity remain ambiguous, it provides some evidence for significant impacts.

Together with nutrient limitation, DA production and accumulation are affected by changes in temperature. Temperature can affect DA production directly by impacting the physiology and metabolism of phytoplankton, but also indirectly, by influencing the presence or absence of specific diatom groups, and by altering the oceanographic context in which blooms develop. *Pseudo-nitzschia* species were found to produce DA in relatively cool and salty waters in the Southern California Bight, during upwelling conditions (Smith et al., 2018). *In situ* measurements found that at temperatures above 19 ºC, *Pseudo-nitzschia* did not produce DA (Smith et al., 2018). However, during the 2014–2015 marine heat wave, also known as the "warm blob", widespread *Pseudo-nitzschia* blooms were observed across the U.S. West Coast (McCabe et al., 2016). It was hypothesized that these blooms were ultimately caused by a temperature increase and shift in ocean circulation associated with this climatic event in Northern California (McCabe et al., 2016). Increased temperature and changing circulation led to more stratified waters and a decrease in nutrient availability, in particular Si concentrations. During this period, under rising temperatures and declining nutrients, DA production initially increased, followed by a decrease as temperature reached levels close to 19 ºC (McCabe et al., 2016). During the same period, a large upwelling event that followed a peak in temperatures further drove DA production levels In Monterey Bay (Ryan et al., 2017). Although the initial induction of toxicity was triggered by rising temperature, its continuation was fueled by anomalous nutrient availability. Thus, temperature may exhibit differing impacts on *Pseudo-nitzschia* blooms and DA production rates, based on the magnitude and direction of the shift in temperature, and interaction with other variables.

DA production responses have also been found to be proportional to light intensity. In general, to sustain DA production, a photon flux density of at least 100 μmol photons m^{-2} s^{-1} is required (Bates et al., 1998). Changing light levels can alter the cellular N preference impacting growth rates and efficiency (Auro and Cochlan, 2013; Hillebrand and Sommer, 1996) and influence the rates of nitrate reduction within cells, resulting in high amounts of available cellular N (Pan et al., 1998). Under nonoptimal light conditions, carbon fixation by *Pseudo-nitzschia* decreases, suggesting that light can exert indirect effects on DA production by controlling the activity of phosphorylation, nitrogen reduction, and carbon assimilation (Pan et al., 1998). However, it is noteworthy that, where nutrient limitation enhances DA production, an increase in light levels proportionally increases DA production.

Because of the complex interactions between physiological and environmental factors, it has been difficult to translate laboratory and *in situ* findings into predictive models of *Pseudo-nitzschia* blooms and DA occurrence in the marine environment. *Pseudo-nitzschia* species diversity adds another layer of complexity. Mechanistic models provide an excellent strategy for representing ecophysiological processes and their physical-biogeochemical drivers within a physically consistent framework. Terseleer et al. (2013) describes one of few studies to employ this approach, where DA production is mechanistically quantified based on changes in nutrients and light levels. The model was adapted to represent *Pseudo-nitzschia* growth and DA production based on the phytoplankton model outlined in Lancelot et al. (1991), by incorporating DA production mechanisms supported by observations (Bates et al., 1998; Bates and Trainer, 2006). Results were validated against batch culture experiments that quantified DA production and DA partitioning between dissolved and particulate phases (dDA and pDA respectively) from *Pseudo-nitzschia* grown at 15 ºC under a light intensity of 120 μmol photons m^{-2} s^{-1} (12:12 h. light: dark cycle) while changing nutrient concentrations (Fehling et al., 2004). The Terseleer et al. (2013) model was able to simulate these batch culture findings and support a mechanistic interpretation for DA accumulation dynamics based on cellular resource allocation. This model provides a starting point for understanding the complex nature of physiological interactions that lead to DA production. Here, we use the Terseleer et al. (2013) model as a comparison for our novel mechanistic model approach.

This mechanistic model is ideally fit to be embedded within more complex three-dimensional (3-D) physical-biogeochemical models that are commonly used to simulate phytoplankton dynamics under realistic oceanic conditions, in particular in coastal settings, integrating a variety of environmental drivers that range from circulation, to temperature, light, nutrients, and grazing (Deutsch et al., 2021; Fennel et al., 2006; Fiechter et al., 2014; Kessouri et al., 2020; Testa et al., 2014). Developing a generalizable realistic 3-D model of *Pseudo-nitzschia* would enable a mechanistic understanding of DA production and accumulation under a range of environmental conditions and stressors. However, 3-D coupled physical-biogeochemical models are computationally expensive, and the inclusion of multiple additional tracers increases their computational burden, especially in high-resolution costal implementations. Thus, it is desirable to develop mechanistic models while limiting the number of additional tracers and the computational complexity (see also Galbraith et al., 2015).

The goal of this paper is to develop a simplified model of *Pseudo-nitzschia* dynamics and DA production that can be easily coupled to realistic 3-D physical-biogeochemical ocean models. We undertake the following steps: (1) summarize experimental data from new chemostat cultures to find statistical relationships between environmental conditions and DA production by *Pseudo-nitzschia*, and to inform modeling; (2) incorporate DA as a secondary metabolite in an existing phytoplankton model, and constrain it with observations, simplifying the

insights of Terseleer et al. (2013); and (3) investigate our novel DA production formulation using model sensitivity experiments under a range of environmental forcings. We build on a variety of previous studies showing a positive relationship between DA production and nutrient stress, primarily Si, and light intensity. We develop a simplified implementation of DA dynamics as part of the Biogeochemical Elemental Cycling (BEC) model (Moore et al., 2002), an ocean ecosystem model that is widely used for global and regional biogeochemical studies, including along the U.S. West Coast (Deutsch et al., 2021; Kessouri et al., 2021, 2020; Moore et al., 2002). Relative to the work by Terseleer et al. (2013), we simplify the multi-compartment approach to only represent DA species rather than multiple precursor metabolite and structural pools, and parameterize the nutrient-limitation DA-producing trigger to be consistent with an extended set of laboratory observations. This simplification allows us to maintain compatibility with BEC's phytoplankton dynamic formulation, which has been tested under a variety of large-scale and regional oceanographic applications (Deutsch et al., 2021; Kessouri et al., 2021; Kessouri et al., 2020; Moore et al., 2002), and to reduce the computational burden for future 3-D simulations. Ultimately, our goal is to enhance HAB predictive capability under varying physical dynamics, and allow exploration of HAB response to complex scenarios of environmental variability, such as anthropogenic nutrient inputs and future climate change (Kessouri et al., 2021; Pan et al., 1998; Trainer et al., 2010).

The rest of the paper is organized as follows. Section 2 describes the numerical model, observational data and analysis used in the paper. Section 3 discusses our model optimization and sensitivity analyses. Section 4 provides a critical assessment of the model results when changing single and multiple environmental parameters. Lastly, Section 5 discusses model caveats and potential applications, and concludes the paper.

2. Material and methods

We designed a flexible modeling framework to predict *Pseudo-nitzschia* DA production and accumulation consisting of physical and biological modules that allows for the translation of laboratory cultures or *in situ* environmental conditions via empirical and mechanistic relationships (Fig. 1). The biological module simulates the dynamics of *Pseudo-nitzschia* and DA production as a function of seawater nutrient concentrations, light, temperature, and other potential drivers. It consists of a version of the BEC model (Moore et al., 2004a,b) updated to represent DA production and accumulation, referred to as BEC-HAB thereafter. We also implement a biological module based on that of Terseleer et al. (2013), which serves as a comparison. Alternative ecological formulations can be readily implemented within our flexible modeling framework.

The physical module specifies the environmental characteristics of the numerical experiments to be conducted, e.g., duration, medium properties such as nutrient concentrations, water flow, temperature, and light. To reproduce laboratory experimental conditions, we implement both batch and chemostat culture setups, although more complex configurations can be designed, e.g., an oceanic mixed layer (Evans et al., 1985).

We use the model to: (1) reproduce prior experiments with batch cultures (Fehling et al., 2004; Terseleer et al., 2013); (2) optimize DA production in BEC-HAB based on a series of new chemostat observations; and (3) investigate the sensitivity of DA production to environmental drivers in the new model formulation.

2.1. Laboratory data

We use previously published results from batch cultures and new laboratory observations from chemostats to constrain and validate the model. Batch cultures were described in Fehling et al., 2004. In the batch cultures, *Pseudo-nitzschia* was grown in seawater enriched with f/2 medium nutrients, with modifications to allow for Si and P limitation. Batch cultures ran for 21 days at 15°C under a 12:12 hr. light: dark cycle (120 μmol photons m^{-2} s^{-1}). Domoic acid, chlorophyll, and nutrient concentrations were measured from culture samples daily. pDA was calculated as the difference between total and dDA. Chlorophyll was

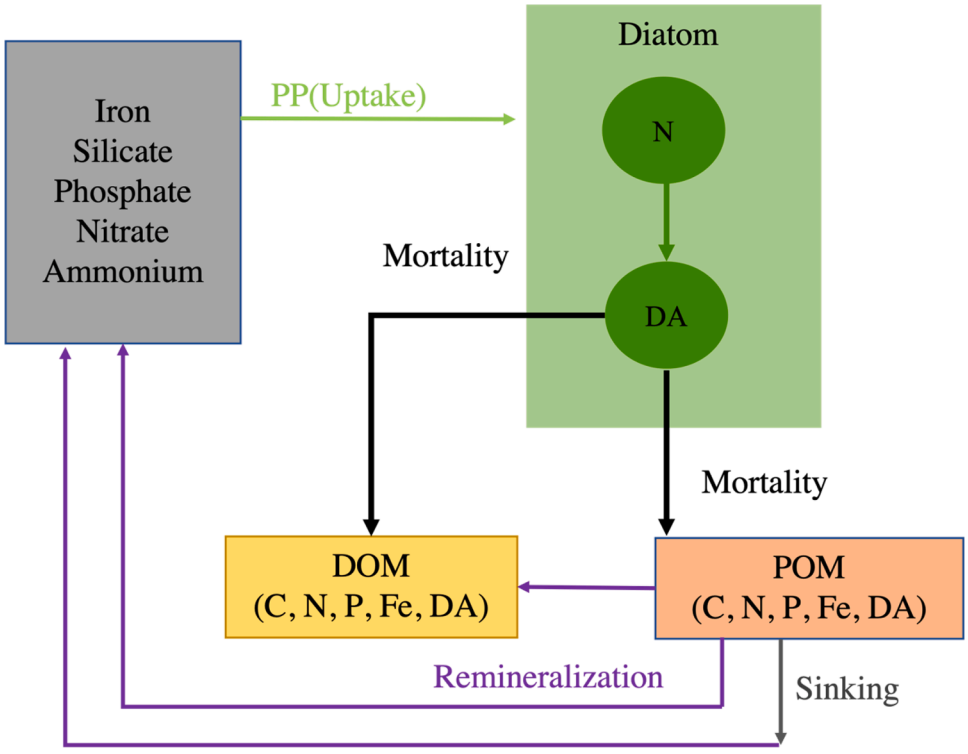

Fig. 1. Simplified DA formulation model schematic. The new DA formulation is part of a version of the BEC model (Moore et al., 2002; 2004a,b) adapted to represent *Pseudo-nitzschia* mono-specific laboratory cultures. BEC accounts for carbon (C), nitrogen (N), phosphorus (P), and iron (Fe). In diatoms (dark green circles), we account for all macronutrients in terms of N primarily, followed by a conversion to domoic acid (DA). Black arrows represent mortality and losses. Purple arrows represent remineralization steps. The green arrow represents primary production (PP) and uptake. The gray arrow represents sinking.

estimated based on a conversion factor for the functional and structural apparatus, using a 0.24 mg Chl a: mmol C ratio from laboratory experiments.

A series of chemostat culture experiments were conducted in the Kudela lab at UC Santa Cruz between June 1999 and June 2000. In the chemostat cultures, *Pseudo-nitzschia* was grown in seawater enriched with f/2 nutrients, with modifications to allow for Si and N limitation. Here, we focus on 36 distinct chemostat experiments for which effluent nutrient, chlorophyll, and DA concentrations (both pDA and dDA) were measured. Experiments were run in 750 ml Plexiglas water-jacketed cylindrical chemostat vessels and were maintained at 100 μmol photons m^{-2} s^{-1} (24 hr. light) at 15°C. Daily monitoring for cell density was accomplished using fluorescence and cellular counts. The chemostats were run at variable dilution rates, which were calculated daily by measuring the effluent volume collected from the vessels. After reaching steady state, samples were collected for measurements of DA, fluorescence, pigments, macronutrients, biogenic silica, and particulate carbon, hydrogen, and nitrogen. Concentrations of pDA were determined using the FMOC-HPLC method described by Pocklington et al. (1990). Samples of dDA below the detection limit were set to zero. When measured, dissolved concentrations were typically less than 40% of the total DA, which is consistent with average field-measured proportions of dDA to total DA in the Southern California Bight (Umhau et al., 2018).

2.2. Mathematical model

2.2.1. Biological module

Terseleer model (TERS). The Terseleer et al. (2013) model, TERS hereafter, is an idealized mathematical model of *Pseudo-nitzschia* growth and DA production based on the AQUAPHY phytoplankton model (Lancelot et al., 2005, 1991), which represents phytoplankton growth and mortality as a function of light, temperature, and nutrients. Terseleer et al. (2013) adapted this model for *Pseudo-nitzschia* by including four cellular compartments, or functional structures, each represented as a separate state variable: the monomeric precursors for macromolecule synthesis, storage products in the form of polysaccharides and lipids, the structural and functional macromolecules, and the internal DA pool. The total biomass of *Pseudo-nitzschia* is represented by the sum of each functional structure. DA production is proportional to the concentration of monomeric precursors and reduced under N limitation. Excretion and cell lysis both release dDA into the environment. Further details on the equations, parameters, and model results can be found in Terseleer et al. (2013).

BEC—HAB model. We built the *Pseudo-nitzschia* biomass and DA production model on the BEC marine ecosystem model (Moore et al., 2002; 2004a,b). BEC provides an idealized representation of primary production and related biogeochemical cycles driven by small, large, and diazotrophic phytoplankton. Large phytoplankton depend on silicon, and thus represent diatoms. BEC reproduces patterns of primary production, export, silica production, chlorophyl, macronutrient and dissolved iron concentrations (Moore, 2004). Nutrient (nitrate, phosphate, silicic acid, and iron) uptake is calculated based on phytoplankton requirements. Photosynthesis and photoacclimation follow the formulation of Geider et al. (1996). The formulation assumes that the light-harvesting apparatus and energy storage respond simultaneously to changes in light. Under low light conditions, biosynthesis is driven by products from the light-harvesting apparatus, whereas under high light conditions, biosynthesis is driven by energy storage molecules (Geider et al., 1996). Dissolved organic matter (DOM) is represented by a semi-labile pool which is remineralized into inorganic nutrients. Following cell mortality, a fraction of the organic matter goes into the dissolved pool, and the rest is placed in the particulate organic matter (POM) pool, which we represent as an explicit tracer in our formulation. POM is remineralized into dissolved inorganic nutrients (Fig. 1).

The starting point for our work is a version of BEC developed to represent biogeochemical cycles along the U.S. West Coast (Deutsch et al., 2021). Our specific implementation includes nutrients and *Pseudo-nitzschia* biomass cycling, here following BEC formulation for diatoms. Compared to the standard BEC formulation (Moore et al., 2002, 2004a), we only include dissolved inorganic nutrients (nitrate, ammonium, phosphate, silicate, iron), diatom biomass, diatom chlorophyll, and particulate organic detritus. We represent both new and recycled primary production, respectively based on nitrate and ammonium, release of dissolved organic matter, mortality and aggregation into particulate organic matter, and remineralization of inorganic nutrients. To simulate mono-specific *Pseudo-nitzschia* lab cultures, we ignore other living functional groups represented by BEC (e.g., picophytoplankton, diazotrophs, zooplankton), as well as the dynamics of the inorganic carbon system, oxygen, and nitrite.

To simulate the cycle of DA, we implement a DA component for diatoms, here *Pseudo-nitzschia* (DiDA; mmol m^{-3} DA), and the two detrital pools (pDA and dDA for particulate and dissolved DA respectively; mmol m^{-3} DA). The equations and parameters for all components except DA are the same as BEC, as documented in previous publications (Moore et al., 2002, 2004a,b). For DA, we start from the following conservation equations describing the evolution of the three DA pools (DiDA, Equation 1; dDA, Equation 11; and pDA, Eq. (14)):

$$\frac{dDiDA}{dt} = DiDA_{prod} - DiDA_{loss} \tag{1}$$

DiDA production is directly dependent on the photosynthetic rate of *Pseudo-nitzschia*, which is proportional to the growth rate (μ; h^{-1}) and the *Pseudo-nitzschia* biomass (*DiN*):

$$DiDA_{prod} = \alpha \cdot \mu \cdot DiN \tag{2}$$

The factor alpha (α) is a stoichiometric conversion term (in units of mol DA: mol DiN) that encapsulates the relationship between production of DA and production of new biomass by diatoms. We assume that this term is a function of the nutrient limitation state of *Pseudo-nitzschia*, according to the empirical equation:

$$\alpha = \beta \times \left[1 - \min\left(\frac{\left[vDi_{PO_4^{3-}}, vDi_{Fe}, vDi_{Si}\right]}{vDi_{NO_3^-} + vDi_{NH_4^+}}, 1\right)\right]^{\gamma} \tag{3}$$

Where vDi_X are Michaelis-Menten-like nutrient limitation terms, with X representing alternatively NO_3^- (mmol m^{-3}), NH_4^+ (mmol m^{-3}), PO_4^{3-} (mmol m^{-3}), Fe (mmol m^{-3}), and Si (mmol m^{-3}). The nutrient limitation terms are calculated as follows:

$$vDi_{NO3} = \frac{\frac{NO_3^-}{K_{NO3}^-}}{1 + \left(\frac{NO_3^-}{K_{NO3}}\right) + \left(\frac{NH_4^+}{K_{NH4}}\right)} \tag{4}$$

$$vDi_{NH4} = \frac{\frac{NH_4^+}{K_{NH4}^+}}{1 + \left(\frac{NO_3^-}{K_{NO3}}\right) + \left(\frac{NH_4^+}{K_{NH4}}\right)} \tag{5}$$

$$vDi_{PO4} = \frac{PO_4^{3-}}{\left(PO_4^{3-} + K_{PO4}\right)} \tag{6}$$

$$vDi_{Fe} = \frac{Fe}{(Fe + K_{Fe})} \tag{7}$$

$$vDi_{Si} = \frac{Si}{(Si + K_{Si})} \tag{8}$$

The nutrient limitation term in the equation for α encapsulates the increase of DA production under stress by nutrients except nitrogen; β sets the maximum ratio of DA to biomass production; and γ is a shape parameter that modulates the rate at which DA production declines as the levels of nutrients other than N increase. The half-saturation constants in the nutrient limitation terms are the same as for nutrient uptake (in units of mmol m^{-3}). A plot of the α term as a function of NO_3^- and Si

(assuming that other nutrients are not limiting) is shown in Fig. 2 for a reference value of $\gamma = 1$.

DiDA loss is dependent on the dynamic cellular stoichiometric quota of DA to DiN (Q_{DADiN}) and the mortality rate:

$$DiDA_{loss} = Q_{DADiN} \cdot J_{Lysis} \tag{9}$$

with the mortality rate (J_{Lysis}) given by:

$$J_{Lysis} = l_{Mort,Di} \cdot DiN. \tag{10}$$

where $l_{Mort,Di}$ is the lysis due to diatom mortality (in units of d^{-1}). Note that diatom mortality releases organic matter and DA into particulate and dissolved forms. Accordingly, the conservation equation for dissolved DA is:

$$\frac{ddDA}{dt} = dDA_{prod} - dDA_{loss} \tag{11}$$

Here, production comes from cell lysis, with a fraction ϕ (here 95%) of mortality allocated to the dissolved DA component:

$$dDA_{prod} = \varphi \cdot Q_{DADiN} \cdot J_{Lysis} \tag{12}$$

We assume that dDA loss follows a constant degradation rate, proportional to BEC's dissolved organic matter remineralization rate ($r_D = 0.01\ d^{-1}$):

$$dDA_{loss} = r_D \cdot dDA. \tag{13}$$

Lysed cells also produce particulate DA, which is calculated based on the following conservation equation:

$$\frac{dpDA}{dt} = pDA_{prod} - pDA_{loss} \tag{14}$$

Here, pDA production comes from the remaining fraction $1 - \varphi$ (here 5%) of lysed cells, i.e., $DiDA_{loss}$:

$$pDA_{prod} = (1 - \varphi) \cdot Q_{DADiN} \cdot J_{Lysis} \tag{15}$$

Finally, pDA loss is proportional to BEC's particulate organic matter remineralization rate ($0.05\ d^{-1}$):

$$pDA_{loss} = r_P \cdot pDA, \tag{16}$$

which is five times higher than the remineralization rate of the semi-refractory dissolved form.

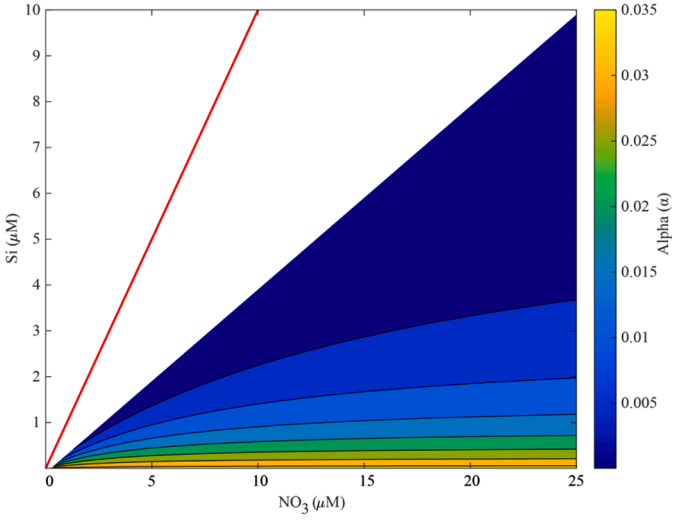

Fig. 2. Plot of the stoichiometric conversion term between DA and *Pseudo-nitzschia* biomass, α, in mol DA: mol DiN as a function of macronutrient concentrations (Si and NO_3^-). The solid red line is the one-to-one line. See Eq. (3) for the mathematical formulation of this term.

2.2.2. Physical module

The physical module of our model provides a representation of the environmental conditions and setup used to run the numerical experiments. Here, we represent batch and chemostat cultures. We use both experimental types to determine the impact of dynamics on DA. The physical module sets the water flow, light, and temperature conditions throughout the experiments. Both experiment types have the same light and temperature levels. The control light level is 13 μmol m^{-2} s^{-1} with continuous light (24 hr.) and the temperature is set to 15 °C. The only difference between the batch and chemostat setups is the presence of a continuous flow at a dilution rate that can be specified in the chemostat case. This flow introduces media into the cultures (i.e., seawater and dissolved nutrients), and removes dissolved and suspended constituent from the culture, including nutrients, living cells, and dissolved and particulate DA at the same specific rate. The control dilution rate is 0.34 d^{-1}, and is adjusted in other simulations to reproduce specific chemostat experiments. The physical and biological modules are coupled and integrated forward in time from a set of initial conditions that match the laboratory experiments. The model is run to equilibrium in the chemostat case (generally achieved after a few model weeks, depending on the dilution rate), or until the end of the laboratory experiments in the batch case.

2.3. Optimization approach

In the version of BEC used for this work, diatom parameters are tuned to provide a match to observations of surface nutrient, chlorophyll, and primary production along the U.S. West Coast (Deutsch et al., 2021). Thus, the diatom functional group should be considered representative of an average diatom community for the Eastern North Pacific. It follows that, while the model formulation should be suitable to represent *Pseudo-nitzschia* dynamics, some of the original parameters may need to be modified to represent monoculture laboratory experiments. Here, we compare two versions of BEC-HAB. The first adopts the original U.S. West Coast BEC diatom parameters, with optimized DA-production parameters only (i.e., β and γ in Eq. (3)). In the second, 11 selected parameters describing diatom growth and mortality are optimized against chemostat observations to allow a better match to *Pseudo-nitzschia* cultures (Table 1).

In both cases, the optimization is carried out by using the covariance matrix adaptation evolution strategy (CMA-ES, Hansen, 2006), which has been previously adopted to constrain marine ecosystem models (Kriest et al., 2017). The CMA-ES is a stochastic approach for numerical optimization of non-linear continuous equations used when multiple parameters need to be optimized simultaneously. Observations from 36 chemostat experiments, including nutrients, chlorophyll, and DA, are used for the optimizations, using a weighted mean square error as the cost function:

$$cost = \frac{\Sigma(\mathbf{se}\ w_i)}{\Sigma(w_i)} \tag{17}$$

Here, the variables used to calculate the cost are macronutrients (PO_4^{3-}, NO_3^-, and Si), chlorophyll from diatoms (Chl), and DA (Table 2). For the calculation of the square errors (se), variables are normalized by their respective observed range from the chemostat experiments. The square errors are further modulated by variable-dependent weights w_i, to give slightly more emphasis to chlorophyll and DA in the cost function (Table 2).

2.4. Sensitivity tests

To determine the sensitivity of DA production in BEC-HAB, we performed two sets of numerical experiments, the first testing the sensitivity to model parameters and the second to environmental variables. These tests allow us to characterize and quantify the indirect and direct effects of environmental changes on DA production and lay the basis for

Table 1
List of the main model parameters investigating in this study, with parameter notation, description, and influence of *Pseudo-nitzschia* physiology and DA production.

Parameter Name	Parameter Notation	Units	Influence
Beta: Maximum rate of DA production	β	mol DA: mol N	DA (p + d)
Gamma: DA production as a function of nutrient limitation	γ	No unit	DA (p + d)
Maximum growth rate of diatoms	$\mu_{max,\ Di}$	h^{-1}	Chl
Light attenuation of diatoms	$a_{Light,\ Di}$	mmol N / (mg Chl W/m^{-2} d^{-1})	Chl
Cellular quota of nitrogen: chlorophyll	$Q_{N:Chl,\ Di}$	mol N: mol Chl	Chl
Lysis of Diatoms	$l_{Mort,Di}$	d^{-1}	DA (p + d), Nutr (POM), Chl
Cellular Si:N	$r_{Si:N}$	mol Si :mol N	Nutrient uptake and cellular quota
Maximal cellular Si:N	$r_{Si:N,\ max}$	mol Si :mol N	Nutrient uptake and cellular quota
Minimal cellular Si:N	$r_{Si:N,\ min}$	mol Si :mol N	Nutrient uptake and cellular quota
Half Saturation of NO_3^-	K_{NO3}	mmol NO_3 m^{-3}	Nutrient uptake
Half Saturation of Si	K_{Si}	mmol Si m^{-3}	Nutrient uptake

Table 2
Parameters used to define the cost function used for the model optimization and relative weights.

Cost parameter	Parameter weight
PO_4^{3-}	0.5
NO_3^-	1
Si	1
Chl	2
pDA	2
dDA	1

interpreting results from the BEC-HAB model in future 3-D implementations with much higher environmental heterogeneity.

2.4.1. Parameter sensitivity experiments

The parameter sensitivity experiments examine how DA production and partitioning are influenced by shifting a single parameter above and below its optimized value (Table 3). For these experiments, we vary each parameter independently to cover a range of approximately one order of magnitude around the optimized value. Accordingly, we first calculate 21 equidistant values by multiplying the optimized value by three to get the maximum value and dividing it by three to get the minimum value. We then hold all other parameters static, adjust the varying parameter, and conduct a full run to estimate the change in DA production and partitioning between dissolved and particulate phases. To evaluate the strength of the response in DA production to each parameter, we calculate the parameter sensitivity response, s_X, as the relative change in DA concentration divided by the relative change in the parameter selected, following:

$$s_X = \frac{X}{DA}\cdot\frac{\Delta DA}{\Delta X} \quad (18)$$

Here, X is the central (i.e., optimized) value of the specific parameter tested, DA is the central DA concentration (i.e., the sum of all DA forms), and Δ indicates the variation around the central value. This variation is estimated from the sensitivity experiments by taking the difference between the first experiment above and the first experiment below the central parameter value. In the following, we describe the rationale for each set of parameter sensitivity experiments. A list of parameters, central values, ranges, and sensitivities for this set of experiments are shown in Table 3.

Table 3
List of the main parameters for the 11-BEC-HAB model optimization, their prior and optimized values, the range for the optimization, and their sensitivity response (s_X) for DA production (defined as the ratio between the relative change in DA production and the relative change in the parameter, see Eq. (18)).

Parameters	Non-optimized value	Optimized value	Sensitivity Range (all run under Si-limitation)	DA production sensitivity response (s_X)
β	0.0137	0.0047	0.0047/3-0.0047×3	1.000
γ	2	0.6667	0.6667/3-0.6667×3	0.2164
$\mu_{Max,Di}$	0.0312	0.0938	0.0938/3-0.0938×3	1.2061
$a_{Light,Di}$	0.0017	0.0012	0.0012/3-0.0012×3	0.4290
$Q_{N:Chl,Di}$	4.0	6.5735	6.5735/3-6.5735×3	0.4205
$l_{Mort,Di}$	0.0062	0.0208	0.0208/3-0.0208×3	0.9441
$r_{Si:N}$	1.0	3	3/3-3 × 3	0.8949
K_{NO3}	2.5	3	3/3-3 × 3	0.0018
K_{Si}	1	1.2393	1.2393/3-1.2393×3	0.0127

We conduct a total of six parameter sensitivity experiments. First, we adjust four parameters independently ($a_{Light,Di}$, $Q_{N:Chl,Di}$, $\mu_{Max,\ Di}$, and $l_{Mort,Di}$). An increase in the maximal growth rate would influence the rate of primary metabolism. A decrease in the rate of light attenuation from the light harvesting apparatus ($a_{Light,Di}$) can establish a positive relationship with DA production, due to decreasing primary metabolism. The cellular quota of nitrogen to chlorophyll ($Q_{N:Chl,Di}$) links the nutrient availability with biomass and primary metabolism. Finally, the specific lysis mortality rate of diatoms ($l_{Mort,Di}$) affects both biomass accumulation and release of DA into the environment.

Second, to assess the effect of nutrient limitation on DA production, we vary the half saturation constants for nutrient uptake (K_{Si} and K_{NO3}) individually. Note that we focus on Si and NO_3^- only, for which we have chemostat observations. Nutrient limitation is determined based on the accessibility of macronutrients uptake into the cell, growth, and metabolism. The value of the half saturation constants will inversely impact the bioavailability of nutrients, i.e., a larger half saturation constant will lead to more intense limitation at low nutrients. Therefore, increasing the half saturation constant for Si could more easily result in Si limitation, which would trigger DA production. Conversely, increasing the half saturation constant for NO_3^- would result in N limitation, which would inhibit DA production.

2.4.2. Environmental sensitivity experiments

To address the impacts of a changing environment, we performed two sets of numerical experiments where we simultaneously vary nutrients, light, and dilution rates. The first set examines the impact of nutrients, by varying Si and NO_3^- simultaneously. The second set examines the interacting impacts of nutrients with light or dilution rate. Although we cannot extrapolate laboratory experiments to *in situ* responses, we can use the results to elucidate relationships between environmental factors and DA production that may be expressed in the marine environment.

For the nutrient limitation experiments, we varied Si and NO_3^- concentrations based on the range realized in the chemostat range (0.001-200 mmol m^{-3}). While the higher end of this range is unrealistic for typical oceanic conditions, the lower end encompasses oligotrophic to

eutrophic oceanic waters. For example, typical surface nutrient concentrations along the California Coast, where DA HABs are commonly observed (Anderson et al., 2006; Kudela and Chavez, 2004; Smith et al., 2018), are generally between 0.1 and 20 mmol m^{-3}.

Light impacts phytoplankton physiology (Geider et al., 1996). High light intensity has been shown to expand the energy storage reserves while condensing the light-harvesting apparatus and vice versa under low light levels. An energy storage shift will affect the cellular quotas of carbon, nitrogen, and silicon within diatoms. In BEC, light modulates the photosynthetic rate, and controls photo-acclimation, driving changes in the cellular Chl to nutrient quotas. For these experiments, we vary light intensity from 20 to 400 μmol photons m^{-2} s^{-1}.

In chemostat experiments, nutrient concentrations and phytoplankton biomass adjust in such a way that the growth rate (i.e., the specific production of new biomass) matches the dilution rate once equilibrium conditions are reached. Thus, the dilution rate provides a powerful way to explore variations in DA production over a range of growth conditions. We also expect additional interacting effects between the growth rate and nutrient availability. For example, studying the impact of Si limitation across a range of growth rates could highlight potential relationships and thresholds for DA production that implicitly and explicitly exist in our model formulation.

3. Results

We divided our results into three sections. Section 3.1 compares model results to observations from batch and chemostat experiments. This comparison includes the TERS model as a reference, and two versions of BEC-HAB. First is the 2-BEC-HAB version, where parameters directly controlling DA production are optimized, and the second (11-BEC-HAB) version, where nine additional *Pseudo-nitzschia* parameters are optimized (Table 1). Note that the TERS model was tuned with batch culture data, while the BEC-HAB models are optimized against chemostat data. Comparison of both formulations under different experimental setups (batch and chemostats) can highlight specific model differences that would not be evident with a more limited comparison. Sections 3.2 and 3.3 discuss the response of *Pseudo-nitzschia* biomass and DA concentration in BEC—HAB's to selected model parameters and environmental conditions.

3.1. Optimized parameters in BEC-HAB

Here we discuss results for the 2- and 11- BEC-HAB optimizations (Table 3). In 2-BEC-HAB, the parameters β and γ directly control the maximum DA production rate and its sensitivity to nutrient limitation. In 11-BEC-HAB, nine additional parameters control nutrient uptake, growth rates, sensitivity to light and nutrient, and chlorophyll synthesis. Results are shown as change (%) relative to the non-optimized BEC-HAB parameter values.

While we do not have strong priors for the parameters β and γ, we find that the optimization consistently converges to specific values. The stoichiometric ratio β stabilizes to 0.062 mol DA: mol N, a value that is well within the optimization range. However, γ tends to decrease to the bottom of the optimization range (0.67), suggesting a weak sensitivity of DA production to nutrient limitation (see discussion in Section 3.3). Note, however, that the range for γ is poorly constrained.

Generally, biological parameters that control diatom growth and biomass accumulation show the largest change relative to the original values in the 11-BEC-HAB optimization. The lysis mortality ($l_{Mort,Di}$) shows the largest change, with a 235% increase (from 0.0062 to 0.0208 mmol m^{-3} N h^{-1}). The maximal growth rate ($\mu_{Max,Di}$) and the stoichiometric ratio of Si:N ($r_{Si:N}$) both increase by 200%. Proportional changes in cellular stoichiometric ratios are estimated as growth increases due to the positive response in the synthesis of proteins and lipids. The nitrogen: chlorophyll quota of diatoms ($Q_{N:Chl,Di}$) increases by 64% from the 2-BEC—HAB model (from 4.0 to 6.57 mol N: mol Chl).

Other parameters change far less in the 11-BEC-HAB optimization. Compared with our 2-BEC-HAB model, β decreases by 25% (from 0.0063 to 0.0047 mol DA: mol N), and γ remains the same (0.67). Our light level is set at 120 μmol photons m^{-2} s^{-1} (12:12 h. light:dark cycle). The light harvesting parameter ($a_{Light,Di}$), which controls photoacclimation, does not greatly change, decreasing by 29% (from 0.0017 to 0.0012 mmol m^{-3} N h^{-1}).

Although the BEC model tracks Si, N, P, and Fe as limiting nutrients, here we focus on the effects of Si and N limitation, for which culture data are available. Accordingly, we optimize parameters that control Si and N uptake, including the $r_{Si:N}$, $r_{Si:N,min}$ and $r_{Si:N,max}$ ratios. The range of $r_{Si:N}$ narrows, with $r_{Si:N,min}$ decreasing by 50% (from 0.50 to 0.25 mol Si: mol N) and $r_{Si:N,max}$ decreasing by 21% (from 5.0 to 3.95 mol Si: mol N). As discussed in Section 2.4.1, the half-saturation constants influence the overall concentrations and responses of Si and N to changing culture conditions. The half saturation constant for Si (K_{Si}) and NO_3^- (K_{NO3}) increased respectively by 24% (from 1 to 1.24 mmol Si m^{-3}) and 20% (from 2.5 to 3.0 mmol N m^{-3}).

3.2. Nutrients, chlorophyll, and DA production

3.2.1. Batch cultures

Comparison of the 2-BEC-HAB model with batch cultures (Fehling et al., 2004) can capture the overall dynamics of biomass bloom, nutrient drawdown, and bloom demise, followed by an increase of DA production in both dissolved and particulate phases (Fig. 3). The ability of the model to reproduce these patterns with two optimized parameters is comparable to that of the more complex model by Terseleer et al. (2013), which was tuned against the batch data, although some discrepancies remain.

First, the 2-BEC-HAB model shows a slight overestimate of chlorophyll concentrations (Fig. 3A), possibly reflecting a combination of higher growth rate, lower mortality, and higher chlorophyll to carbon ratios. However, nutrient drawdown follows a trajectory that is close to observations (Fig. 3B-D), suggesting realistic uptake rates. Second, 2-BEC-HAB significantly underestimates DA production, both in the particulate and dissolved form (Fig. 3E-F). Although these results are based on Si limitation over P limitation, similar DA trajectories reflect the general dependence of DA production on nutrient limitation. Note that the 2-BEC-HAB model is not specifically tuned to batch culture data, whereas the TERS model is. Thus, it is not surprising that the TERS model matches batch observations more closely than our model. The underestimate of DA in the 2-BEC-HAB thus suggests a higher DA production ability (i.e. the stoichiometric ratio β) for the *Pseudo-nitzschia* strains in the Fehling et al. (2004) batch cultures relative to the strains in the chemostat experiments.

3.2.2. Chemostat cultures

Comparison of BEC-HAB simulations with chemostat observations shows that the models can capture the general dynamics of *Pseudo-nitzschia* growth and DA production under a broad range of dilution rates and nutrient limitations (Fig. 4). The overall performance of the 2-BEC-HAB is comparable to that of the TERS model, with somewhat less accurate representation of chlorophyll, and better representation of DA. In contrast, and not surprisingly, the performance of the 11-BEC-HAB is markedly better than both the 2-BEC-HAB and the TERS model. A detailed analysis of chlorophyll, nutrients and DA reveals important factors behind the different performances of the three model formulations.

Chlorophyll concentration is a good proxy for how well the model reproduces growth and other cellular mechanisms that lead to diatom biomass accumulation in the cultures. In the TERS and 2-BEC-HAB models, we observe many instances in which the final chlorophyll concentrations drop to zero, indicating that, contrary to the observations, growth rates cannot match the high dilution rates under the prescribed experimental conditions. However, this is different in the 11-

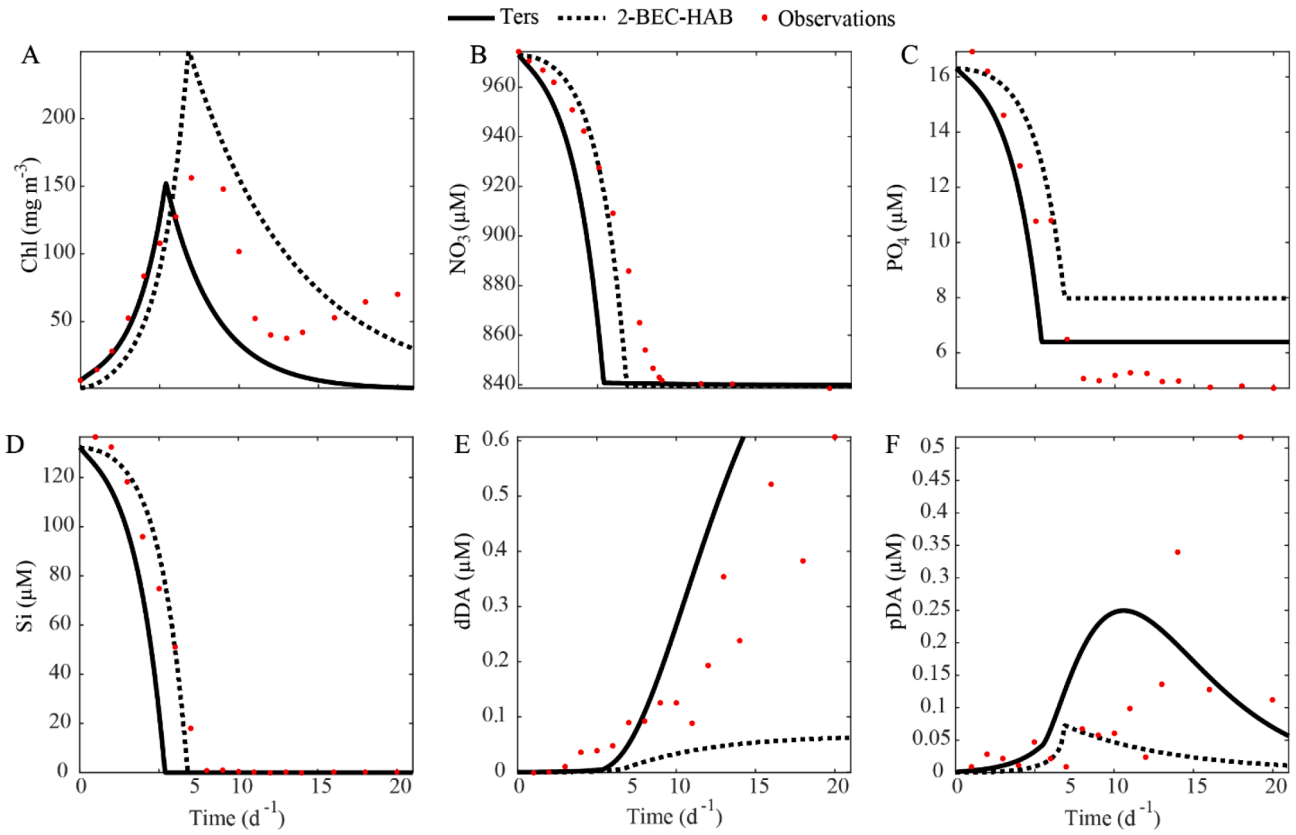

Fig. 3. Model comparison against Fehling et al. (2004) batch culture observations. A. Chlorophyll concentrations. B. Nitrate (NO_3^-) concentrations. C. Phosphate (PO_4^{3-}) concentrations. D. Silicate (Si) concentrations. E. Dissolved domoic acid (dDA) concentrations. F. Particulate domoic acid (pDA) concentrations. Red dots show observations from Fehling et al. (2004) lab experiments. Solid black line represents TERS model output. Dotted black line represents 2-BEC-HAB model output.

BEC-HAB model, which can sustain high dilution rates upwards of 1.3 d^{-1}. The inability of the TERS model to sustain high levels of chlorophyll accumulation is likely due to differences in *Pseudo-nitzschia* strains between the batch and chemostat cultures, as discussed in Section 3.2.1. Likewise, the 2-BEC-HAB model, which uses parameters tuned for an average oceanic diatom, fails to sustain viable *Pseudo-nitzschia* populations at high dilution rates. Instead, higher values of maximum growth rate in the 11-BEC-HAB model allow it to maintain realistic chlorophyll and biomass across the experimental range in dilution rates. Consequently, the TERS model captures 11% of the variability in observed chlorophyll, whereas the 2-BEC-HAB model only captures around 7%. However, the 11-BEC-HAB model improves this match to 44%. In both BEC-HAB versions, the model somewhat underestimates chlorophyll under N limitation, and overestimates it under Si limitation, at lower dilution rates (Fig. 4D and G), a behavior that is further discussed at the end of this section.

Comparison of nutrient concentrations reveals similar patterns of model performance. Although there are small improvements in NO_3^- between the BEC-HAB models, we see a dramatic improvement in Si (Fig. 4B, E, H). The TERS and 2-BEC-HAB model capture approximately 26 and 25% of the variability of chemostat data respectively, while the 11-BEC-HAB model increases to 77%. This improvement reflects the ability for the 11-BEC-HAB model to simulate realistic Si nutrient drawdown under high dilution rates compared with the inefficient Si nutrient uptake and in turn lower sustained growth in the TERS and 2-BEC-HAB models.

Relative to the TERS model, both the 2- and 11-BEC-HAB formulations significantly improve the performance of DA production, both in terms of absolute values and correlation with the experiments (Fig. 4C, F, I). This performance is highest for the 11-BEC-HAB model, which reproduces 73% and 62% of the variance of particulate and dissolved DA, reflecting improvement in both growth rates and *Pseudo-nitzschia* biomass. Additionally, improved Si concentrations allow the model to capture a more realistic DA production across experiments. An important difference with the TERS model is that, under N limitation, our DA formulation does not allow any DA production, while TERS does. Accordingly, multiple chemostat experiments show small concentrations of DA production even under N limited conditions, mainly in the particulate pool, which is captured by the more complex TERS formulation.

To test the ability of the models to reproduce differences between N and Si limited chemostats, we ran two simple sensitivity experiments with the 11-BEC-HAB model, varying dilution rates (as a proxy for growth rate) and Si limitation (as a proxy for general nutrient limitation) (Fig. 5). In the chemostat experiments, growth rates and chlorophyll show a positive relationship as the dilution rate increases, until a maximum is reached, after which concentrations drop off (Fig. 5A). This peak in chlorophyll is observed at higher dilution rates under N limitation (near 1.2 d^{-1}), and lower dilution rates under Si limitation (near 0.3 d^{-1}). This potentially reflects earlier onset of Si limitation driven by high Si *Pseudo-nitzschia* requirements, and adjustments in the cellular Chl: N elemental ratio driven by the type of limiting nutrient. The 11-BEC-HAB model can capture this behavior, indicating a correct representation of the relationship between dilution rate, nutrient uptake, and chlorophyll production.

Similarly, in the chemostat experiments, the 2-BEC-HAB model reproduces the positive relationship between Si limitation and DA synthesis (Fig. 5B). Observations show that at high Si limitation, DA production and α are high – a pattern reproduced by the model. However, observations show more variability than the model. Furthermore, the experiments are characterized by slightly more intense Si limitation than reproduced by the model, which in turn correspond to the highest

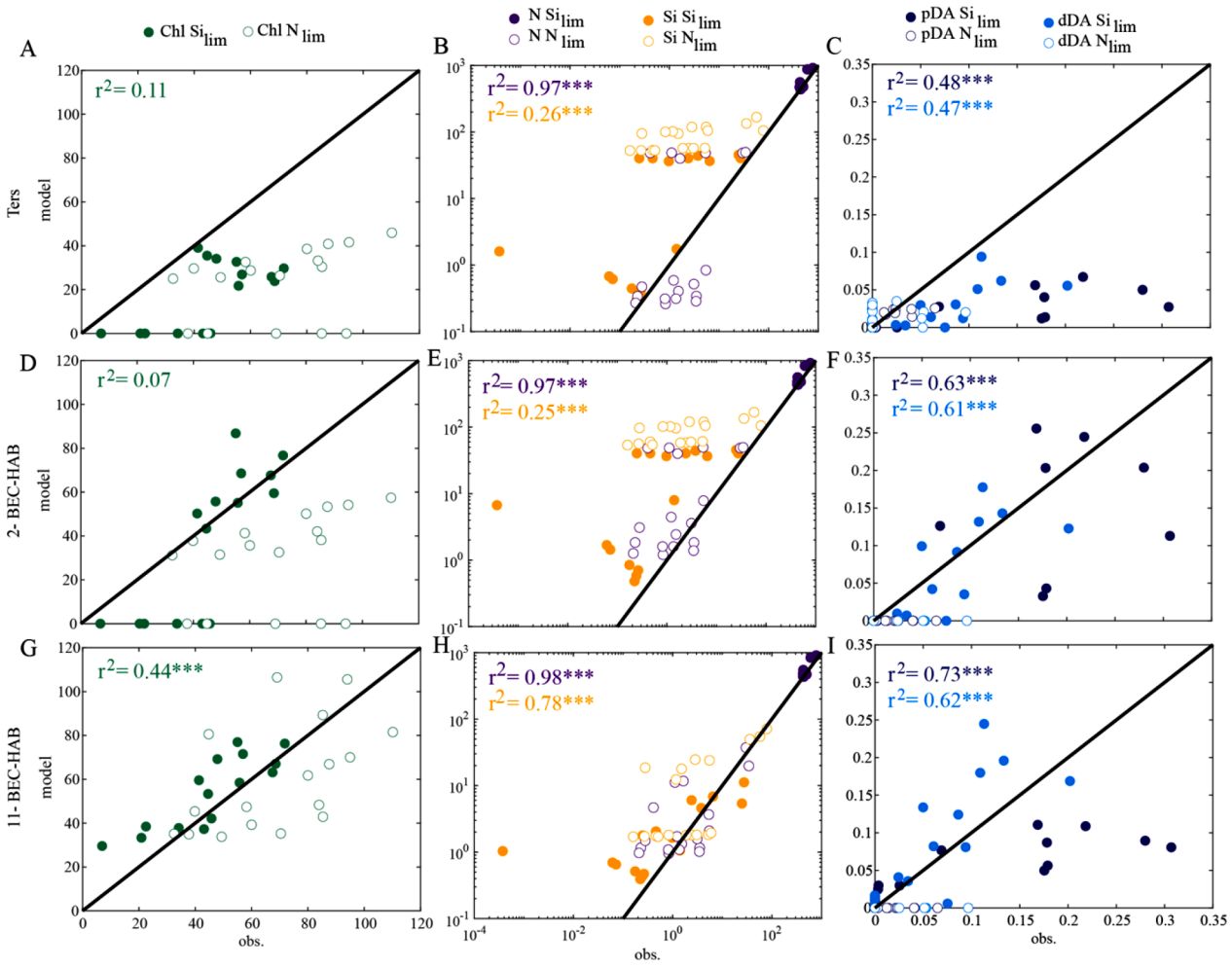

Fig. 4. Model comparison against chemostat ($n = 36$) experimental observations. A-C. TERS model output against observed chlorophyll (A), macronutrients (B), and domoic acid (C) concentrations from chemostat experiments. D-E. Same as (A-C) but for 2-BEC-HAB model output. G-I. Same as (A-C) but for 11-BEC-HAB model output. Solid filled circles represent Si limited experiments, whereas open circles represent N limited experiments. Solid black lines show the one-to-one match. The r^2 values are calculated using Pearson correlation coefficients. Statistically significant r^2 are shown by asterisks (*); *p-value<0.05, **p-value <0.01, ***p-value <0.001.

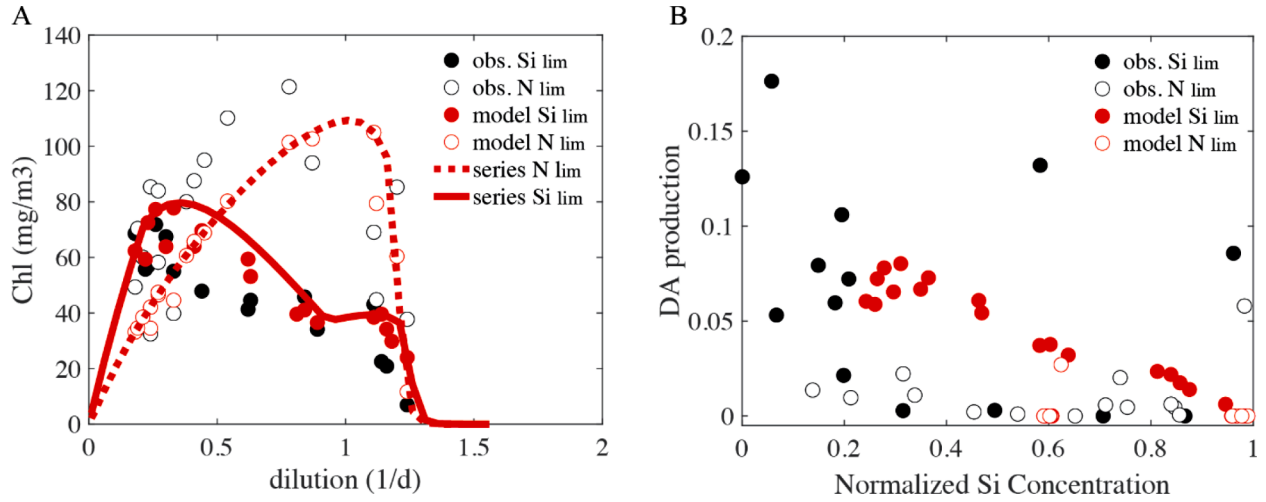

Fig. 5. 11-BEC-HAB model sensitivity to dilution rate and nutrient limitation. A. Chlorophyll concentration as a function of dilution rate. B. Increased DA production with increased Si limitation (normalized Si = Si/ (Si + K_{Si})) values closer to 0). Black colors represent chemostat experiment observations. Red colors represent 11-BEC-HAB model output. Filled circles show Si limited chemostats and open circles show N limited. The continuous red lines in A show an average series of chemostat experiments with typical Si-limited (solid line) and N-limited (dashed line) conditions, for which dilution rates are continuously varied between 0 and 2 d^{-1}.

DA production rates observed. This underestimate of Si limitation (see also Fig. 3E and F) thus results in a reduction of DA production in the Si limited experiments, producing biases in DA concentrations, especially in the particulate form, shown in Fig. 4I.

3.3. Sensitivity to model parameters

We characterize the model sensitivity to specific parameters by comparing the relative change in DA production for a given relative change in model parameter value, encapsulated by the sensitivity response s_X (Eq. (18) and Table 3). Values of s_X close to one represent a perfectly linear sensitivity – i.e., a doubling of the parameter would cause a doubling of DA production rates. Conversely, values higher than one indicate a strong sensitivity, and values lower show a weak sensitivity. As an extreme case, a sensitivity response of zero indicates no sensitivity of DA production to that specific parameter. The response of

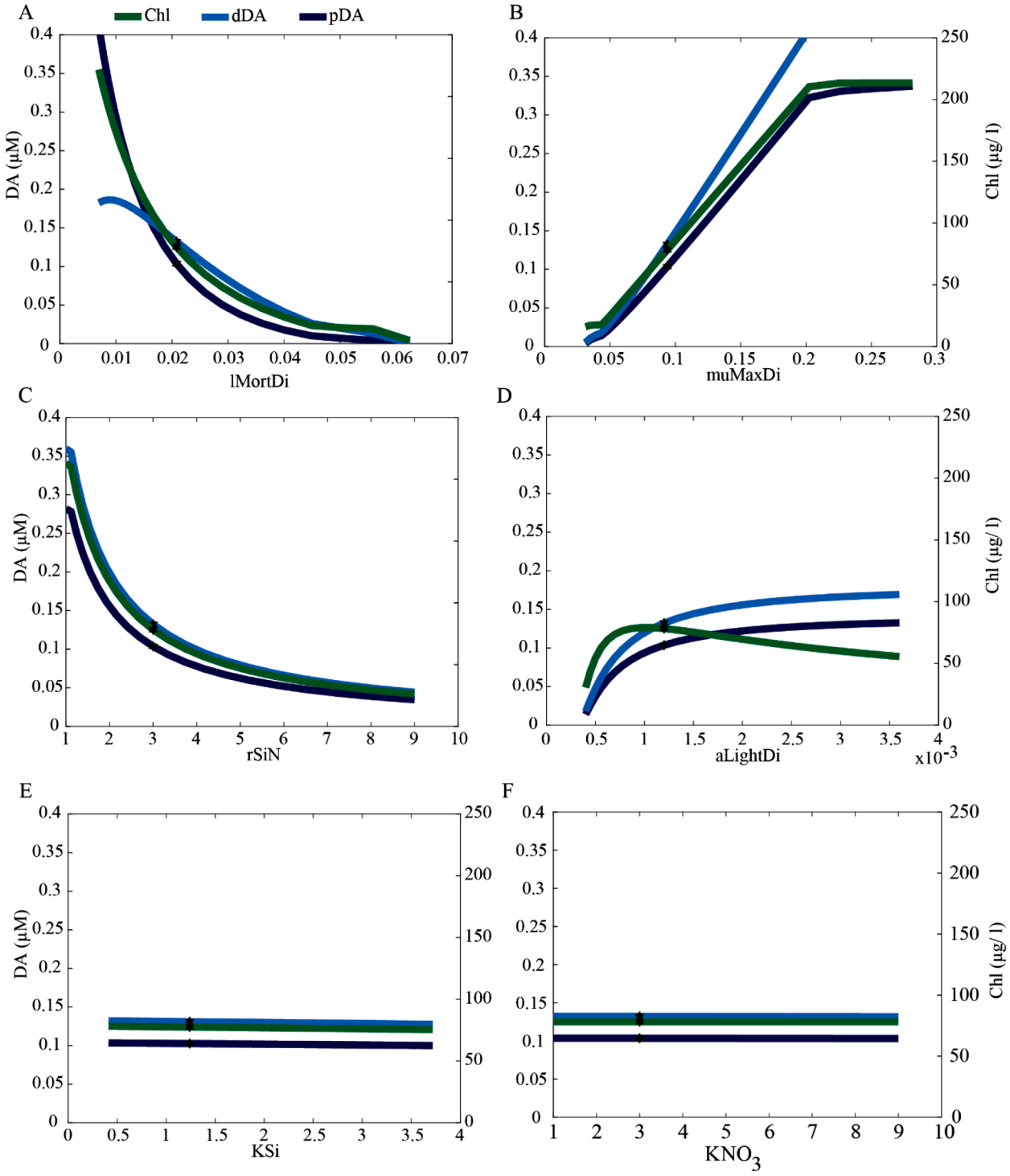

Fig. 6. Parameter sensitivity response in the 11-BEC-HAB model to DA and chlorophyll. A. Sensitivity to the specific lysis rate ($l_{Mort,Di}$). B. Sensitivity to the maximum growth rate ($\mu_{max,\ Di}$). C Sensitivity to cellular the Si:N ratio ($r_{Si:N}$). D. Sensitivity to the strength of the photosynthetic light response ($a_{light,\ Di}$). E. Sensitivity to silica limitation K_{Si}. F. Sensitivity to nitrogen limitation K_{NO3}. Dark blue represents particulate domoic acid (pDA), light blue represents dissolved domoic acid (dDA), and green represents chlorophyll concentrations (Chl). Black star represents the optimized value for each parameter.

the model to the range of values tested is shown in Fig. 6.

First, lysis mortality of diatoms shows the largest relative percent change in DA production. We found that this parameter, unsurprisingly, is also our most sensitive (Fig. 6A). Generally, we found a decreasing trend of biomass and DA, both dissolved and particulate, with increasing mortality. The similar response of these quantities indicates that mortality acts to reduce the viable diatom biomass that can be maintained in the chemostats for a given dilution rate, in turn reducing the rates of new biomass production and DA proportionally. At the highest mortality level tested, no viable diatom populations can be maintained. Note that at the optimal value for lysis mortality, the rate of pDA production is two times lower than the rate of dDA production. Furthermore, the decrease in the dDA production is more gradual, although its change spans that of pDA concentrations.

Although the maximal growth rate and the $r_{Si:N}$ ratio produce a change in DA concentration with similar magnitude (3-fold change), they exhibit opposite patterns (Fig. 6B and C). As the maximum growth rate increases, diatom biomass and DA concentration increase. The increase is linear across most of the range in growth rates but shows a saturation for the particulate components at the highest rates. Partitioning of pDA and dDA is similar, but, as the growth rate increases, pDA increases somewhat faster, and does not show saturation at the highest growth rate. Changes in $r_{Si:N}$ produce a decline in diatom biomass and DA production, but do not alter the proportion between pDA and dDA (Fig. 6C). The decrease in biomass and DA production with increasing silica requirements reflect progressive Si limitation of the chemostat cultures as Si is incorporated into diatom frustules and removed from the culture medium.

The last highest sensitivity is $a_{Light,Di}$. We found increasing concentrations of DA with equal partitioning between dissolved and particulate phases as $a_{Light,Di}$ increased, with a saturation towards the upper values (Fig. 6D). The range in DA produced is 0.13 mmol m^{-3}, significantly less than the other biological parameters. Intriguingly, the chlorophyll curve exhibits a maximum at relatively low values of $a_{Light,Di}$, peaking at approximately 80 μg Chl L^{-1}, which also corresponds to our optimized value.

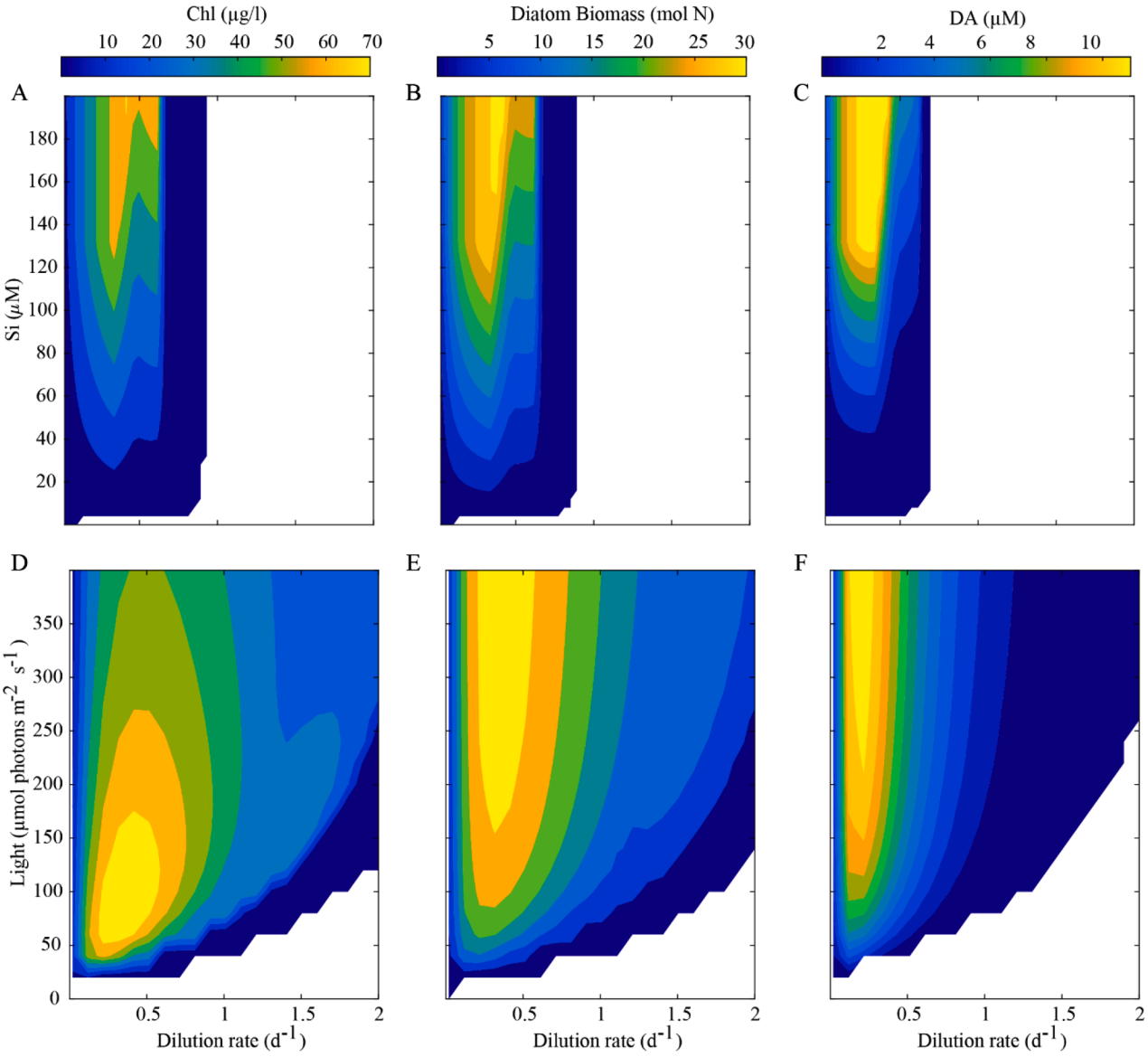

Fig. 7. Environmental sensitivity in 11-HAB-BEC model to changing macronutrients, light, and dilution rate. A-C represent the effect of Si (μM) and dilution rates (d^{-1}) when NO_3^- (μM) and light (μmol photons m^{-2} s^{-1}) are kept constant at 561 μM and 99.96 μmol photons m^{-2} s^{-1}; and D-F represent the effects of light (μmol photons m^{-2} s^{-1}) and dilution rates (d^{-1}) when Si (μM) and NO_3^- (μM) are kept constant at 45 and 561 μM. The first column represents the response in Chl; the second column represents the response in diatom biomass (mol N); and the last column represents the response in total DA (μM).

K_{Si} and K_{NO3} show the lowest sensitivity of all our parameters (Fig. 6E and F). We find that a minor negative relationship exists between K_{Si} (K_{NO3}) and DA production, such that as K_{Si} (K_{NO3}) increases the DA production decreases slightly. This minimal sensitivity is reflected in the behavior of chlorophyll and is likely caused by the relatively high Si concentration achieved in the chemostat configuration (1.7 mmol m^{-3}), which, even under Si limited conditions, never reaches concentrations significantly lower than the K_{Si} tested.

3.4. Sensitivity to environmental factors

The dilution rate, by setting the overall growth rate of a chemostat viable population, directly impacts *Pseudo-nitzschia* biomass and DA production. However, for a given growth rate, these quantities are also modulated by nutrient and light limitation.

Fig. 7A-C shows the impact of changing dilution rate under a range of Si concentrations. (Note that NO_3^- is never limiting in these experiments.) Under Si limitation, at all severities, *Pseudo-nitzschia* growth cannot be sustained at rates higher than approximately 1.2 divisions d^{-1} in the model. The highest biomass (~110 μg Chl L^{-1}) is produced at a growth rate of 0.3 divisions d^{-1} at the highest Si concentration. This high biomass accumulation results in chlorophyll concentrations as high as 350 μg Chl L^{-1} and a total DA accumulation of 47 mmol m^{-3}. By increasing the severity of Si limitation, *Pseudo-nitzschia* biomass is proportionally reduced. Further, we find that the partitioning of DA into pDA and dDA is not uniform.

Under Si limitation, the interaction between dilution rate and light intensity produced nonlinear relationships in *Pseudo-nitzschia* biomass, chlorophyll, and DA production (Fig. 7D-F). We found moderate to high concentrations of *Pseudo-nitzschia* biomass at relatively low dilution rates (0.12-0.71 d^{-1}) and moderate light intensity (60-200 μmol photons m^{-2} s^{-1}). Within this intersecting range, the chlorophyll concentration is high (~75 μg Chl L^{-1}). However, the highest biomass is found at a dilution rate of 0.3 d^{-1} with light levels above 100 μmol photons m^{-2} s^{-1}. Comparatively, high DA production within this interaction is rather limited. Generally, we find maximum DA production centered around 0.3 d^{-1} and light levels above 45 μmol photons m^{-2} s^{-1}. Although our model shows an optimal level of *Pseudo-nitzschia* and DA accumulation at relatively low dilution rates, DA production under Si limitation can be maintained across a large parameter space and is unconditionally enhanced by light availability.

4. Discussion

Simulations under batch and chemostat setups indicate that the BEC model, coupled with a simple nutrient-dependent DA production formulation, can effectively represent observed DA production. The main parameter controlling the cellular DA synthesis quota, β, appears to be relatively well constrained by the optimizations to the chemostat data, and, as expected, affects linearly the total DA production (sensitivity equal to 1 in Table 3). However, the limited sensitivity demonstrated by γ indicates a general weak response to the shape of the nutrient limitation curve (Eq. (3)). This is mirrored by a weak response of DA production to the half-saturation constants for nutrient limitation – at least under the chemostat conditions tested here. This limited influence is shown by the low values for the sensitivity responses for γ and K_{Si} listed in Table 3, and by the negligible response of both chlorophyll and DA concentrations to changes in the half saturation constant shown in Fig. 6E. It is possible that DA production is triggered by Si limitation but not substantially modulated by the degree of limitation, i.e., once Si limitation is established, DA production quickly saturates to its maximum cellular rate. Despite this weak sensitivity, our simple DA formulation (Eq. (3)) can still reproduce the positive relationship between Si limitation and DA production.

The simplified BEC-HAB model reproduces a realistic dynamic for *Pseudo-nitzschia* growth and DA production across a range of experimental conditions. Analysis of the HAB-BEC model performance against batch and chemostat data reveals aspects of the model behavior that compare favorably with observations, while highlighting remaining biases. First, we highlight the model ability to reproduce the partitioning of DA between dissolved and particulate phases without specific tuning. The chemostat experiments show a somewhat similar partitioning into the two phases with an average value of 2 pDA:dDA (Fig. 4), similar to that found in observations (Fehling et al., 2004). There is variation among the three model configurations, with the 11-BEC-HAB model producing the smallest pDA:dDA partitioning (1.47) and 2-BEC-HAB the largest (2.67). Batch culture experiments show somewhat higher partitioning, with an average between models of 6 pDA:dDA (Fig. 3). This difference may reflect the fact that chemostat experiments are run to equilibrium with constant conditions, while the batch experiments encompass the exponential growth, stationary phase and the decay phase of the bloom, and phytoplankton are thus exposed to variable nutrient concentrations and relative limitation. Other studies show that the amount of dDA released by *Pseudo-nitzschia* cells can be controlled by physiological processes as well as environmental stressors (Hagström et al., 2011). However, we note that estimates of the release of dDA from *Pseudo-nitzschia* cells can differ greatly in other *in situ* experimental studies (Delegrange et al., 2018).

Second, the model requires a relatively high cellular Si:N quota, which in turn exerts an important influence on DA production. The chemostat experiments and the optimized model suggest large Si:N requirement (~3 mol Si: mol N) of *Pseudo-nitzschia* cells, as compared to more typical diatoms (~ 1:1 mol Si: mol N). The Si:N requirement of *Pseudo-nitzschia* in a continuous laboratory experiment was found to range on average from 0.66 to 2 mol Si: mol N depending on the Si within the media (Pan et al., 1996). In general, *Pseudo-nitzschia* is known to have light silicification primarily in its frustules (Lundholm et al., 2002). However, Si is not only found in the frustules, but it is also stored in the cell where it is utilized for DNA production (Brzezinski et al., 1990; Pan et al., 1996). The high requirement found in the chemostat experiments suggests that *Pseudo-nitzschia* may have the ability to uptake dissolved Si effectively, potentially resulting in relatively rapid establishment of Si limitation and Si stress. Since the Si:N cellular quota affects DA production through metabolism (Marchetti and Harrison, 2007; Martin-Jézéquel et al., 2000), the increased Si:N requirement could explain why Si limitation shows one of the strongest impacts on DA production both in field and laboratory studies. However, we note that laboratory experiments tend to be less variable than field observations, likely because of more uniform conditions.

In the 11-HAB-BEC model, light results in a proportional change in DA production. A minimum light level is necessary to sustain growth and DA production through photosynthesis (Bates et al., 1991; Pan et al., 1998). The highest *Pseudo-nitzschia* growth rates have been observed at 100 μmol photons m^{-2} s^{-1} (Bates et al., 1998). Much research has shown inconsistent links with DA production, with changes in light increasing, decreasing, or leaving DA production unchanged (Cusack et al., 2002; El-Sabaawi and Harrison, 2006). However, strain-specific experiments showed that *P. granii* biomass increased at light levels between 20 and 150 μmol photons m^{-2} s^{-1} (El-Sabaawi and Harrison, 2006). In our model, biomass does increase with increasing light; however, the lowest light level that sustains viable biomass is around 45 rather than 20 μmol photons m^{-2} s^{-1} under typical nutrient availability (Fig. 7D and E). This discrepancy may be caused by differences in experimental set ups, or differences in *Pseudo-nitzschia* species and strains between different studies and highlights the importance of both factors to capturing underlying biological mechanisms. Light also affects DA production. When grown at light levels of 115 μmol photons m^{-2} s^{-1}, *P. australis* was found to produce 24 to 130 times more DA than when grown at 12 μmol photons m^{-2} s^{-1} (Cusack et al., 2002). Our model does show a large sensitivity across this light range. However, the model does not sustain biomass at 12 μmol photons m^{-2} s^{-1} unlike these experiments (Fig. 7D-F).

Our model generates a peak in DA concentrations at moderate dilution rates. In the model, increasing the dilution rate ramps up DA concentration until an optimal rate, then decreases it (Fig. 7F). This pattern is followed by both chlorophyll and *Pseudo-nitzschia* biomass (Fig. 7D and E). At low dilution (growth) rates, the chemostats equilibrate at low concentrations of the limiting nutrient, here Si, resulting in low accumulation of biomass, chlorophyll and DA. As the dilution rate continues to ramp up, supporting an increasing inflow of nutrients, the specific growth rate also increases, and more biomass, chlorophyll and DA can accumulate. As nutrient saturation is reached, the growth rate stops increasing, following the Michaelis-Menten dynamics governing nutrient limitation. At this point, nutrients and growth rates are close to their maximum values, but as the dilution rates continue to increase, biomass begins to decline, reflecting increasing removal from the culture. Changing dilution (growth) rate has been shown to affect DA concentrations in lab experiments (Bates et al., 1998; Pan et al., 1996; Thessen et al., 2009; Trainer et al., 2012). Under Si limited chemostat experiment, *P. multiseries* produced more cellular DA per division in slow growing conditions compared with rapid ones (Bates et al., 1996). Additional laboratory experiments with *P. multiseries* under Si-limited conditions showed that increased growth rates resulted in a decrease in DA production both in batch and chemostat cultures (Pan et al., 1998; 1996). Ultimately, while Si limitation is the main trigger for DA production, dilution and growth rates have significant impacts on the amount of DA that can accumulate in the environment.

Comparison of the model performance against different experimental datasets shows that, after optimization against the chemostat data, the model captures the overall dynamics of *Pseudo-nitzschia* growth and DA production of batch experiments reasonably well, while underestimating the total amount of DA accumulating in the cultures. This suggests that species and strain-specific physiological differences are likely important, e.g., the stoichiometry of DA synthesis relative to new biomass fixation. While *Pseudo-nitzschia* has a cosmopolitan distribution (Hasle, 2002; Trainer et al., 2012), not all strains have been documented to produce DA (Lelong et al., 2012; Silver et al., 2010). DA producing strains generate variable toxin levels based on species, growth/biomass, and environmental conditions. The enormous range of variability in pDA concentrations observed in the ocean can be in part explained by large differences in growing conditions. Laboratory experiments can generate values as low as 2.9 10^{-5} pmol/cell (Cerino et al., 2005), whereas measurements in field samples can reach 0.25 pmol/cell or higher (Trainer et al., 2000). As such, species and strain diversity are highly important in determining growth rates, cellular stoichiometry, and DA production capabilities. These characteristics may need to be identified on a regional basis before implementing models at specific locations.

Diversity within *Pseudo-nitzschia* strains can impact mechanistic predictability. Although DA concentrations of various *Pseudo-nitzschia* strains in culture appear to change under nutrient stress (Bates et al., 1991; Pan et al., 1996), laboratory conditions do not always accurately reflect field observations. Our model validation was conducted using multiple experimental datasets. The batch cultures of Fehling et al. (2004), used to compare the HAB-BEC model to the TERS model, employed *P. seriata*, a typical cold-water species found throughout the upper water column and at the interface of sea ice (Hasle, 2002). In contrast, the chemostat experiments utilized multiple strains of *P. multiseries* and *P. australis*, most common along the U.S. West Coast in relatively warm and nutrient-rich surface waters. *P. seriata, P. australis*, and *P. multiseries* are typically found in very different locations and environmental conditions but have all been found to produce DA during periods of nutrient stress.

We highlight three main caveats to our study. First, although experimental data suggests that N limitation allows the accumulation of small concentrations of DA, primarily in the dissolved form (Fig 4C, F, I), our model is designed to shut down DA production under N limited conditions. N limitation is most common in oligotrophic open ocean waters, but less common in nitrate-rich coastal waters, e.g., upwelling-dominated California Current where *Pseudo-nitzschia* is often found. Laboratory data show that N limitation can stress the cell and increase the Si quota, potentially driving the cell into further stress (Pan et al., 1998, 1996). Cellular stress in turn fosters production of secondary metabolites such as DA. In our model, DA production stops when cells are N limited. Thus, BEC-HAB is unable to produce the low levels of DA observed in the N limited chemostat experiments (Fig. 4F, I). In contrast, the TERS model produces DA that is directly proportional to the availability of cellular DA precursors, which are proportional to photosynthesis times a N limitation term, and thus only stop when dissolved inorganic N concentrations drop to zero, and N limitation is complete (Terseleer et al., 2013). Note that other laboratory experiments have also found DA production under N limitation (Calu et al., 2009; Kudela and Chavez, 2004). It is also possible that rapid cycling of NH_4^+ (or dissolved organic nitrogen) contributes to these observations. *Pseudo-nitzschia* has little preference for N sources, and can uptake and utilize NH_4^+ as a nitrogen source to produce DA (Auro and Cochlan, 2013). However, we do not represent rapid NH_4^+ cycling in our experiments, because of the lack of dedicated $NH4^+$ measurements that would allow to constrain it. While we opted for a simple but relatively effective formulation, improvements may be required in the future to capture low levels of DA production under incomplete N limitation, together with better understanding of the mechanistic response to the effects of N availability, including its form, and possible consequences for DA speciation.

Our second caveat is that we only tested the model under constant light conditions, and thus did not investigate the role of the duration of light-replete vs. dark conditions. Photoperiod has been shown to impact the photosynthetic process, with longer periods of light requiring less nutrient uptake and enabling better energy storage (Geider et al., 1996). Fehling et al. (2004) found greater amounts of DA produced under a longer photoperiod. This supports both the hypothesis that photosynthetic energy is required for DA production but also that energy can be stored and used during dark periods. Although sensitivity to light levels varies between and within *Pseudo-nitzschia* strains, it also provides insights into patterns and mechanisms of DA production that could be incorporated into models, such as energy or metabolite storage (Terseleer et al., 2013).

The last caveat is that our model does not include DA-producing mechanisms that have been suggested by prior work, but for which dedicated observations are still severely limited. In particular, micronutrients have been shown to impact the growth rate of *Pseudo-nitzschia* and trigger DA production, often giving it a competitive edge relative to other species (Maldonado et al., 2002). However, much research is strain specific, at times leading to contradictory results. Iron deficiency has been shown in certain strains to increase DA production and trigger the release of significant concentrations of dDA into the water column (Maldonado et al., 2002). Yet, other studies have found that iron limitation simply stresses cells too far, to the point of inhibiting DA production (Marchetti et al., 2006; Marchetti and Harrison, 2007). Because the mechanisms driving DA production and micronutrient stress relationships are not well understood, we did not specifically address micronutrient triggers into our model. However, given *Pseudo-nitzschia*'s ability under iron stress to release phytosiderophores into the environment to enhance iron uptake (Rue and Bruland, 2001; Wells et al., 2005), we expect that iron limitation may lead to DA production, especially in the California Current, where iron limitation is frequently tied to circulation patterns (Hogle et al., 2018). Through this process, primary metabolism is slowed, and DA production may be triggered. Intriguing, phytosiderophores can also bind to and favor uptake of copper (McKnight and Morel, 1980; Rue and Bruland, 2001), which has also been linked to increased DA production rates (Wells et al., 2005). Future work is necessary to elucidate the relationship between micronutrient limitation – in particular iron – and DA production, with the goal of developing a mechanistic representation of this process for

inclusion in models.

5. Conclusions

We designed a simplified mechanistic model to demonstrate the triggers, interactions, and patterns of *Pseudo-nitzschia* growth and DA production. Our study also provides new laboratory observations and a general framework to formulating, tuning, and evaluating *Pseudo-nitzschia* growth and DA production models, with the potential for model improvement and incorporation of new processes and data. We show that simple cellular mechanisms represented by our model can accuratelyly produce DA and its variation under different experimental conditions. Our findings show that the optimization of specific biological parameters is in turn important to provide a realistic representation of DA production and accumulation. We have also discussed the impacts of *Pseudo-nitzschia* diversity and its implications for predictability with realistic 3-D ocean models. Because of its simplicity, our formulation can be easily embedded within more complex ocean-ecosystem models to conduct simulations of DA-driven HABs. However, given the sensitivity in DA production to specific triggers shown by our model experiments, regional fine tuning may be necessary for improved realism. The model development and evaluation shown in this study represent preliminary steps towards establishing operational models for DA and HAB prediction based on mechanistic rather than statistical approaches. However, further calibration against *in situ* observations under a variety of conditions would likely be required for robust regional-scale predictions. Future work on additional factors affecting DA production, such as trace metal limitation, changes in seawater pH and CO_2 caused by ocean acidification, or availability of different forms of N, is also required to provide additional insight into *Pseudo-nitzschia* HAB formation and toxin production in a changing ocean.

Declaration of Competing Interest

The authors declare that they have no known competing financial interests or personal relationships that could have appeared to influence the work reported in this paper.

Data Availability

Data will be made available on request.

Acknowledgements

This research was supported by the NOAA under Ecosystem and Harmful Algal Bloom (ECOHAB) Award NA18NOS4780174. This is ECOHAB publication #1028. A. Moreno acknowledges support from the University of California President's Postdoctoral Fellowship. C. Anderson, R. Kudela, and C. Edwards acknowledges California Sea Grant Award #NA10OAR4170060 and seed funding from the Packard Foundation at UC Santa Cruz. D. Bianchi acknowledges computational support by the Extreme Science and Engineering Discovery Environment through allocation TG-OCE170017, and by the supercomputer Hoffman2 at the University of California Los Angeles, at the Institute for Digital Research and Education.

References

Anderson, C.R., Brzezinski, M.A., Washburn, L., Kudela, R., 2006. Circulation and environmental conditions during a toxigenic Pseudo-nitzschia australis bloom in the Santa Barbara Channel, California. Mar. Ecol. Prog. Ser. 327, 119–133. https://doi.org/10.3354/meps327119.

Auro, M.E., Cochlan, W.P., 2013. Nitrogen Utilization and Toxin Production by Two Diatoms of the Pseudo-nitzschia pseudodelicatissima Complex: P. cuspidata and P. fryxelliana. J. Phycol. 49, 156–169. https://doi.org/10.1111/jpy.12033.

Bates, S., de Freitas, A.S., Milley, J.E., Pocklington, R., Quilliam, M.A., Smith, J.C., Worms, J., 1991. Controls on domoic acid produciton by the diatom Nitzschia pungens f. multiseries in culture: nutrients and irradiance. Can. J. Fish. Aquat. Sci. 48, 1136–1144.

Bates, S.S., Garrison, D., Horner, R., 1998. Bloom Dynamics and physiology producing pseudo-Nitzschia species. NATO ASI Ser. G Ecol. 267–292.

Bates, S.S., Hubbard, K.A., Lundholm, N., Montresor, M., Leaw, C.P., 2018. Pseudo-nitzschia, Nitzschia, and domoic acid: new research since 2011. Harmful Algae 79, 3–43. https://doi.org/10.1016/j.hal.2018.06.001.

Bates, S.S., Trainer, V.L., 2006. The ecology of harmful diatoms. Ecol. Harmful Algae 81–93. https://doi.org/10.1007/978-3-540-32210-8_7.

Brzezinski, M., Olson, R., Chisholm, S., 1990. Silicon availability and cell-cycle progression in marine diatoms. Mar. Ecol. Prog. Ser. 67, 83–96. https://doi.org/10.3354/meps067083.

Brzezinski, M.A., 1992. Cell-cycle effects on the kinetics of silicic acid uptake and resource competition among diatoms. J. Plankton Res. 14, 1511–1539. https://doi.org/10.1093/plankt/14.11.1511.

Buck, K.R., 1992. Autecology of the diatom Pseudonitzschia australis, a domoic acid producer, from Monterey Bay, California. Mar. Ecol. Prog. Ser. 84, 293–302. https://doi.org/10.3354/meps084293.

Calu, G., Martin-jezequel, V., Lefau, E., Lassus, P., Weigel, P., Amzil, Z., Phycotoxines, L., Bp, Y., 2009. The influence of nitrogen speciation on growth and toxicity of Pseudo-nitzschia multiseries and P. pungens in batch and continuous cultures. In: 7th Int. Conf. {…} 2001, pp. 1–7.

Cerino, F., Orsini, L., Sarno, D., Dell'Aversano, C., Tartaglione, L., Zingone, A., 2005. The alternation of different morphotypes in the seasonal cycle of the toxic diatom Pseudo-nitzschia galaxiae. Harmful Algae 4, 33–48. https://doi.org/10.1016/j.hal.2003.10.005.

Cusack, C.K., Bates, S.S., Quilliam, M.A., Patching, J.W., Raine, R., 2002. Confirmation of domoic acid production by Pseudo-nitzschia australis (Bacillariophyceae) isolated from Irish waters. J. Phycol. 38, 1106–1112. https://doi.org/10.1046/j.1529-8817.2002.01054.x.

Delegrange, A., Lefebvre, A., Gohin, F., Courcot, L., Vincent, D., 2018. Pseudo-nitzschia sp. diversity and seasonality in the southern North Sea, domoic acid levels and associated phytoplankton communities. Estuar. Coast. Shelf Sci. 214, 194–206. https://doi.org/10.1016/j.ecss.2018.09.030.

Deutsch, C., Frenzel, H., McWilliams, J.C., Renault, L., Kessouri, F., Howard, E., Liang, J. H., Bianchi, D., Yang, S., 2021. Biogeochemical variability in the California Current System. Prog. Oceanogr. 196, 102565 https://doi.org/10.1016/j.pocean.2021.102565.

El-Sabaawi, R., Harrison, P.J., 2006. Interactive effects of irradiance and temperature on the photosynthetic physiology of the pennate diatom Pseudo-nitzschia granii (Bacillariophyceae) from the northeast subarctic Pacific. J. Phycol. 42, 778–785. https://doi.org/10.1111/j.1529-8817.2006.00246.x.

Evans, G.T., Parslow, J.S., Evans, G.T., Parslow, J.S., 1985. A model of annual plankton cycles. Deep Sea Res. Part B. Oceanogr. Lit. Rev. 32, 759. https://doi.org/10.1016/0198-0254(85)92902-4.

Fehling, J., Davidson, K., Bolch, C.J., Bates, S.S., 2004. Growth and domoic acid production by Pseudo-nitzschia seriata (Bacillariophyceae) under phosphate and silicate limitation. J. Phycol. 40, 674–683. https://doi.org/10.1111/j.1529-8817.2004.03213.x.

Fennel, K., Wilkin, J., Levin, J., Moisan, J., O'Reilly, J., Haidvogel, D., 2006. Nitrogen cycling in the Middle Atlantic Bight: results from a three-dimensional model and implications for the North Atlantic nitrogen budget. Global Biogeochem. Cycles 20, 1–14. https://doi.org/10.1029/2005GB002456.

Fiechter, J., Curchitser, E.N., Edwards, C.A., Chai, F., Goebel, N.L., Chavez, F.P., 2014. Global Biogeochemical Cycles of model resolution and coastal topography. Global Biogeochem. Cycles 371–385. https://doi.org/10.1002/2013GB004683.Received.

Galbraith, E.D., Dunne, J.P., Gnandesikan, A., Slater, R.D., Sarmiento, J.L., Dufour, C.O., de Souza, G.F., Bianchi, D., Claret, M., Rodgers, K.B., Sedish Marvasti, S., 2015. Complex fucntionality with minimal computation: promise and pitfalls of reduced-tracer ocean biogeochemistry models. J. Adv. Model. Earth Syst. 548–565. https://doi.org/10.1002/2015MS000463.Received.

Garrison, D.L., Conrad, S.M., Eilers, P.P., Waldron, E.M., 1992. Confirmation of domoic acid production by Pseudonitzschia Australis (Bacillariophyceae) cultures. J. Phycol 28, 604–607.

Geider, R.J., Macintyre, H.L., Kana, T.M., 1996. A dynamic model of photoadaptation in phytoplankton. Limnol. Oceanogr. 41, 1–15. https://doi.org/10.4319/lo.1996.41.1.0001.

Hagström, J.A., Granéli, E., Moreira, M.O.P., Odebrecht, C., 2011. Domoic acid production and elemental composition of two Pseudo-nitzschia multiseries strains, from the NW and SW Atlantic Ocean, growing in phosphorusor nitrogen-limited chemostat cultures. J. Plankton Res. 33, 297–308. https://doi.org/10.1093/plankt/fbq102.

Hansen, N., 2006. The CMA evolution strategy: a comparing review, in: towards a new evolutionary computation, advances on estima- tion of distribution algorithms.

Hasle, G.R., 2002. Are most of the domoic acid-producing species of the diatom genus Pseudo-nitzschia cosmopolites? Harmful Algae 1, 137–146. https://doi.org/10.1016/S1568-9883(02)00014-8.

Hillebrand, H., Sommer, U., 1996. Nitrogenous nutrition of the potentially toxic diatom Pseudonitzschia pungens f. multiseries Hasle. J. Plankton Res. 18, 295–301. https://doi.org/10.1093/plankt/18.2.295.

Hogle, S.L., Dupont, C.L., Hopkinson, B.M., King, A.L., Buck, K.N., Roe, K.L., Stuart, R.K., Allen, A.E., Mann, E.L., Johnson, Z.I., Barbeau, K.A., 2018. Pervasive iron limitation at subsurface chlorophyll maxima of the California Current. Proc. Natl. Acad. Sci. USA 115, 13300–13305. https://doi.org/10.1073/pnas.1813192115.

Kessouri, F., Bianchi, D., Renault, L., McWilliams, J.C., Frenzel, H., Deutsch, C.A., 2020. Submesoscale currents modulate the seasonal cycle of nutrients and productivity in

the California current system. Glob. Biogeochem. Cycles 34, 1–15. https://doi.org/10.1029/2020GB006578.
Kessouri, F., McWilliams, J.C., Bianchi, D., Sutula, M., Renault, L., Deutsch, C., Feely, R. A., McLaughlin, K., Ho, M., Howard, E.M., Bednaršek, N., Damien, P., Molemaker, J., Weisberg, S.B., 2021. Coastal eutrophication drives acidification, oxygen loss, and ecosystem change in a major oceanic upwelling system. Proc. Natl. Acad. Sci. USA 118, 1–8. https://doi.org/10.1073/pnas.2018856118.
Kriest, I., Sauerland, V., Khatiwala, S., Srivastav, A., Oschlies, A., 2017. Calibrating a global three-dimensional biogeochemical ocean model (MOPS-1.0). Geosci. Model Dev. 10, 127–154. https://doi.org/10.5194/gmd-10-127-2017.
Kudela, R.M., Chavez, F.P., 2004. The impact of coastal runoff on ocean color during an El Niño year in central California. Deep. Res. Part II Top. Stud. Oceanogr. 51, 1173–1185. https://doi.org/10.1016/j.dsr2.2004.04.002.
Ladizinsky, N.C., 2003. The Influences of Dissolved Copper On the Production of Domoic Acid By Pseudo-Nitzschia Species in Monterey Bay. laboratory experiments and field observations, California.
Lancelot, C., Spitz, Y., Gypens, N., Ruddick, K., Becquevort, S., Rousseau, V., Lacroix, G., Billen, G., 2005. Modelling diatom and Phaeocystis blooms and nutrient cycles in the Southern Bight of the North Sea: the MIRO model. Mar. Ecol. Prog. Ser. 289, 63–78. https://doi.org/10.3354/meps289063.
Lancelot, C., Veth, C., Mathot, S., 1991. Modelling ice-edge phytoplankton bloom in the Scotia-Weddell sea sector of the Southern Ocean during spring 1988. J. Mar. Syst. 2, 333–346. https://doi.org/10.1016/0924-7963(91)90040-2.
Lelong, A., Hégaret, H., Soudant, P., Bates, S.S., 2012. Pseudo-nitzschia (Bacillariophyceae) species, domoic acid and amnesic shellfish poisoning: revisiting previous paradigms. Phycologia 51, 168–216. https://doi.org/10.2216/11-37.1.
Lundholm, N., Hasle, G.R., Fryxell, G.A., Hargraves, P.E., 2002. Morphology, phylogeny and taxonomy of species within the Pseudo-nitzschia americana complex (Bacillariophyceae) with descriptions of two new species, Pseudo-nitzschia brasiliana and Pseudo-nitzschia linea. Phycologia 41, 480–497. https://doi.org/10.2216/i0031-8884-41-5-480.1.
Maldonado, M.T., Hughes, M.P., Rue, E.L., Wells, M.L., 2002. The effect of Fe and Cu on growth and domoic acid production by Pseudo-nitzschia multiseries and Pseudo-nitzschia australis. Limnol. Oceanogr. 47, 515–526. https://doi.org/10.4319/lo.2002.47.2.0515.
Marchetti, A., Harrison, P.J., 2007. Coupled changes in the cell morphology and elemental (C, N, and Si) composition of the pennate diatom *Pseudo-nitzschia* due to iron deficiency. Limnol. Oceanogr. 52, 2270–2284. https://doi.org/10.4319/lo.2007.52.5.2270.
Marchetti, A., Maldonado, M.T., Lane, E.S., Harrison, P.J., 2006. Iron requirements of the pennate diatom Pseudo-nitzschia: comparison of oceanic (high-nitrate, low-chlorophyll waters) and coastal species. Limnol. Oceanogr. 51, 2092–2101. https://doi.org/10.4319/lo.2006.51.5.2092.
Martin-Jézéquel, V., Hildebrand, M., Brzezinski, M.A., 2000. Silicon metabolism in diatoms: implications for growth. J. Phycol. 36, 821–840. https://doi.org/10.1046/j.1529-8817.2000.00019.x.
McCabe, R.M., Hickey, B.M., Kudela, R.M., Lefebvre, K.A., Adams, N.G., Bill, B.D., Gulland, F.M.D., Thomson, R.E., Cochlan, W.P., Trainer, V.L., 2016. An unprecedented coastwide toxic algal bloom linked to anomalous ocean conditions. Geophys. Res. Lett. 43 https://doi.org/10.1002/2016GL070023, 10,366-10,376.
McKnight, D.M., Morel, F.M.M., 1980. Copper complexation by siderophores from filamentous blue-green algae. Limnol. Oceanogr. 25, 62–71. https://doi.org/10.4319/lo.1980.25.1.0062.
Moore, J.K., 2004. Upper ocean ecosystem dynamics and iron cycling in a global three-dimensional model. Glob. Biogeochem. Cycles 18, 1–21. https://doi.org/10.1029/2004GB002220.
Moore, J.K., Doney, S.C., Glover, D.M., Fung, I.Y., 2002. Iron cycling and nutrient-limitation patterns in surface waters of the World Ocean. Deep Sea Res. Part II Top. Stud. Oceanogr. 49, 463–507.
Moore, J.K., Doney, S.C., Lindsay, K., 2004a. Upper ocean ecosystem dynamics and iron cycling in a global three-dimensional model. Global Biogeochem. Cycles 18. https://doi.org/10.1029/2004GB002220 n/a-n/a.
Moore, J.K., Doney, S.C., Lindsay, K., 2004b. Upper ocean ecosystem dynamics and iron cycling in a global three-dimensional model. Global Biogeochem. Cycles 18.
Pan, Y., Bates, S.S., Cembella, A.D., 1998. Environmental stress and domoic acid production by Pseudo-nitzschia: a physiological perspective. Nat. Toxins 6, 127–135. https://doi.org/10.1002/(sici)1522-7189(199805/08)6:3/4<127::aid−nt9>3.0.co;2-2.
Pan, Y., Subba Rao, D.V., Mann, K.H., Brown, R.G., Pocklington, R., 1996. Effects of silicate limitation on production of domoic acid, a neurotoxin, by the diatom Pseudo-nitzschia multiseries. I. Batch culture studies. Mar. Ecol. Prog. Ser. 131, 225–233. https://doi.org/10.3354/meps131225.
Pocklington, R., Milley, J.E., Batesf, S.S., Bird, C.J., De Freitas, A.S.W., Quilliamt, M.A., 1990. Trace determination of domoic acid in seawater and phytoplankton by high-performance liquid chromatography of the fluorenylmethoxycarbonyl (fmoc) derivative. Int. J. Environ. Anal. Chem. 38, 351–368. https://doi.org/10.1080/03067319008026940.
Rue, E., Bruland, K., 2001. Domoic acid binds iron and copper: a possible role for the toxin produced by the marine diatom Pseudo-nitzschia. Mar. Chem. 76, 127–134. https://doi.org/10.1016/S0304-4203(01)00053-6.
Ryan, J.P., Kudela, R.M., Birch, J.M., Blum, M., Bowers, H.A., Chavez, F.P., Doucette, G. J., Hayashi, K., Marin, R., Mikulski, C.M., Pennington, J.T., Scholin, C.A., Smith, G. J., Woods, A., Zhang, Y., 2017. Causality of an extreme harmful algal bloom in Monterey Bay, California, during the 2014–2016 northeast Pacific warm anomaly. Geophys. Res. Lett. 44, 5571–5579. https://doi.org/10.1002/2017GL072637.
Silver, M.W., Bargu, S., Coale, S.L., Benitez-Nelson, C.R., Garcia, A.C., Roberts, K.J., Sekula-Wood, E., Bruland, K.W., Coale, K.H., 2010. Toxic diatoms and domoic acid in natural and iron enriched waters of the oceanic Pacific. Proc. Natl. Acad. Sci. USA 107, 20762–20767. https://doi.org/10.1073/pnas.1006968107.
Smith, J., Connell, P., Evans, R.H., Gellene, A.G., Howard, M.D.A., Jones, B.H., Kaveggia, S., Palmer, L., Schnetzer, A., Seegers, B.N., Seubert, E.L., Tatters, A.O., Caron, D.A., 2018. A decade and a half of Pseudo-nitzschia spp. and domoic acid along the coast of southern California. Harmful Algae 79, 87–104. https://doi.org/10.1016/j.hal.2018.07.007.
Terseleer, N., Gypens, N., Lancelot, C., 2013. Factors controlling the production of domoic acid by Pseudo-nitzschia (Bacillariophyceae): a model study. Harmful Algae 24, 45–53. https://doi.org/10.1016/j.hal.2013.01.004.
Testa, J.M., Li, Y., Lee, Y.J., Li, M., Brady, D.C., Di Toro, D.M., Kemp, W.M., Fitzpatrick, J.J., 2014. Quantifying the effects of nutrient loading on dissolved O2 cycling and hypoxia in Chesapeake Bay using a coupled hydrodynamic-biogeochemical model. J. Mar. Syst. 139, 139–158. https://doi.org/10.1016/j.jmarsys.2014.05.018.
Thessen, A.E., Bowers, H.A., Stoecker, D.K., 2009. Intra- and interspecies differences in growth and toxicity of Pseudo-nitzschia while using different nitrogen sources. Harmful Algae 8, 792–810. https://doi.org/10.1016/j.hal.2009.01.003.
Trainer, V.L., Adams, N.G., Bill, B.D., Stehr, C.M., Wekell, J.C., Moeller, P., Busman, M., Woodruff, D., 2000. Domoic acid production near California coastal upwelling zones, June 1998. Limnol. Oceanogr. 45, 1818–1833. https://doi.org/10.4319/lo.2000.45.8.1818.
Trainer, V.L., Bates, S.S., Lundholm, N., Thessen, A.E., Cochlan, W.P., Adams, N.G., Trick, C.G., 2012. Pseudo-nitzschia physiological ecology, phylogeny, toxicity, monitoring and impacts on ecosystem health. Harmful Algae 14, 271–300. https://doi.org/10.1016/j.hal.2011.10.025.
Trainer, V.L., Pitcher, G.C., Reguera, B., Smayda, T.J., 2010. The distribution and impacts of harmful algal bloom species in eastern boundary upwelling systems. Prog. Oceanogr. 85, 33–52. https://doi.org/10.1016/j.pocean.2010.02.003.
Umhau, B.P., Benitez-Nelson, C.R., Anderson, C.R., McCabe, K., Burrell, C., 2018. A time series of water column distributions and sinking particle flux of pseudo-nitzschia and domoic acid in the Santa Barbara Basin, California. Toxins 10. https://doi.org/10.3390/toxins10110480.
Wells, M.L., Trick, C.G., Cochlan, W.P., Hughes, M.P., Trainer, V.L., 2005. Domoic acid: the synergy of iron, copper, and the toxicity of diatoms. Limnol. Oceanogr. 50, 1908–1917. https://doi.org/10.4319/lo.2005.50.6.1908.